A&A manuscript no.
(will be inserted by hand later)

Your thesaurus codes are:
06(02.08.1, 08.02.1, 02.14.1, 08.14.1, 13.07.1, 02.05.1)

ASTRONOMY
AND
ASTROPHYSICS
15.10.1996

Coalescing neutron stars – a step towards physical models

II. Neutrino emission, neutron tori, and gamma-ray bursts

M. Ruffert[1⋆], H.-Th. Janka[1⋆⋆], K. Takahashi[1,2⋆⋆⋆], and G. Schäfer[3†]

[1] Max-Planck-Institut für Astrophysik, Karl-Schwarzschild-Str. 1, Postfach 1523, 85740 Garching, Germany
[2] Physik-Department E12, Technische Universität München, James-Franck-Str., 85748 Garching, Germany
[3] Max-Planck-Arbeitsgruppe "Gravitationstheorie", Friedrich–Schiller–Universität, Max-Wien-Platz 1, 07743 Jena, Germany

October 15, 1996

Abstract. Three-dimensional hydrodynamical, Newtonian calculations of the coalescence of equal-mass binary neutron stars are performed with the "Piecewise Parabolic Method". The properties of neutron star matter are described by the equation of state of Lattimer & Swesty (1991) which allows us to include the emission of neutrinos and to evaluate our models for the $\nu\bar{\nu}$-annihilation in the vicinity of the merging stars. When the stars have merged into one rapidly spinning massive body, a hot toroidal cloud of gas with a mass of about 0.1–$0.2\,M_\odot$ forms around the wobbling and pulsating central $\sim 3\,M_\odot$ object. At that time the total neutrino luminosity climbs to a maximum value of 1–$1.5 \cdot 10^{53}$ erg/s of which 90–95% originate from the toroidal gas cloud surrounding the very dense core. The mean energies of ν_e, $\bar{\nu}_e$, and heavy-lepton neutrinos ν_x are around 12 MeV, 20 MeV, and 27 MeV, respectively. The characteristics of the neutrino emission are very similar to the emission from type-II supernovae, except for the $\bar{\nu}_e$ luminosity from the merged neutron stars which is a factor 3–6 higher than the luminosities of the other neutrino species.

When the neutrino luminosities are highest, $\nu\bar{\nu}$-annihilation deposits about 0.2–0.3% of the emitted neutrino energy in the immediate neighborhood of the merger, and the maximum integral energy deposition rate is 3–$4 \cdot 10^{50}$ erg/s. Since the $3\,M_\odot$ core of the merged object will most likely collapse into a black hole within milliseconds, the energy that can be pumped into a pair-photon fireball is insufficient by a factor of about 1000 to explain γ-ray bursts at cosmological distances with an energy of the order of $10^{51}/(4\pi)$ erg/steradian. Analytical estimates show that the additional energy provided by the annihilation of $\nu\bar{\nu}$ pairs emitted from a possible accretion torus of $\sim 0.1\,M_\odot$ around the central black hole is still more than a factor of 10 too small, unless focussing of the fireball into a jet-like expansion plays an important role. A few $10^{-4}\,M_\odot$ of very neutron-rich, low-entropy matter may be dynamically ejected shortly after the neutron stars have merged, and another 10^{-4} up to a few $10^{-2}\,M_\odot$ of strongly neutronized, high-entropy material could be carried away from the accretion torus in a neutrino-driven wind. The contamination with this baryonic material is a severe threat to a relativistic fireball. Aspects of a possible r-processing in these ejecta are discussed.

Key words: gamma rays: bursts – elementary particles: neutrinos – nuclear reactions, nucleosynthesis, abundances – stars: neutron – binaries: close – hydrodynamics

1. Introduction

During the first two and a half years of operation, the Burst and Transient Source Experiment (BATSE) on the Compton Gamma Ray Observatory (GRO) has observed 1122 cosmic gamma-ray bursts (Meegan et al. 1995a). The angular distribution of the bursts on the sky is amazingly well compatible with isotropy (e.g., Tegmark et al. 1995). There are recent claims that a tenuous indication of an association with host galaxies is present in the burst sample evaluated by Larson et al. (1996) and that a correlation with Abell clusters has been found on a 95% confidence level in the BATSE 3B catalog (Kolatt & Piran 1996). If confirmed, these would be the first hints of a correlation of gamma-ray bursts with any other astronomical population. Number counts show a deficiency of faint bursts relative to the $-3/2$ power law expected for the brightness distribution of a homogeneous spatial distribution of standard candle sources (Fenimore 1996). This paucity of weak bursts could be caused by a truncation of the distance to very far burst sources or might be an effect due to the expansion of the universe or could be associated with an evolution of the spatial density of bursts (Bloom et al. 1996). Both observational facts, isotropy

Send offprint requests to: M. Ruffert
⋆ e-mail: mruffert@mpa-garching.mpg.de
⋆⋆ e-mail: thj@mpa-garching.mpg.de
⋆⋆⋆ e-mail: kjt@mpa-garching.mpg.de
† e-mail: gos@gravi.physik.uni-jena.de

and bend in the brightness distribution, would be naturally explained if the gamma-ray bursters were situated at cosmological distances (e.g., Paczyński 1995, Hartmann et al. 1996, Kolatt & Piran 1996). Nevertheless, the assumption that they might populate an extended Galactic halo cannot be ruled out yet (Lamb 1995), and Galactic halo models have been constructed (Podsiadlowski et al. 1995) which are able to fulfill the stringent limits set by the isotropy of the detected bursts and their inhomogeneous spatial distribution.

The distribution of measured gamma-ray burst durations exhibits a bimodal structure with peaks at about 0.5 s and about 30 s (Meegan et al. 1995a). The bursts can be as short as $\sim$ 1 ms but can also last for several 100 s with variabilities and fluctuations on a millisecond time scale (Fishman et al. 1994). The extremely short sub-ms rise times of the gamma-ray luminosities suggest that the energy sources for the bursts must be connected with very compact astrophysical objects which have a typical size of the order of 100 km. This favors neutron stars or black holes as most likely candidates for the enigmatic origin of the cosmic gamma-ray bursts.

Despite of more than 25 years of gamma-ray burst observations, there is neither a convincing identification of counterparts in any other energy range of the electromagnetic spectrum (Greiner 1995a, 1995b; Vrba 1996), nor has a generally accepted, satisfactory theoretical model been developed yet (Nemiroff 1994a, Hartmann & Woosley 1995, Woosley 1996). About 120 gamma-ray burst models have been published in the refereed literature until 1992 (Nemiroff 1994a), until 1994 there were 135 (Nemiroff 1994b), and maybe another one or two dozens have been added since.

Cosmological explanations have become increasingly popular in the more recent publications, a fair fraction of which suggests collisions of two neutron stars or mergers of binaries consisting of either two neutron stars (NS-NS) or a black hole and a neutron star (BH-NS) as possible sources of the bursts (e.g., Paczyński 1986; Goodman 1986; Eichler et al. 1989; Piran 1990; Paczyński 1991; Narayan et al. 1991, 1992; Piran et al. 1992; Mészáros & Rees 1992a,b, 1993; Woosley 1993a; Mochkovitch et al. 1993, 1995a; Hernanz et al. 1994, Katz & Canel 1995a). One of the reasons for the attractivity of these scenarios is the desired compactness of the objects, another reason is the knowledge that these events should happen and should release large amounts of energy (Dermer & Weiler 1995). The frequency of NS-NS and BH-NS mergers was estimated to be between 10^{-6} and 10^{-4} per year per galaxy (Narayan et al. 1991, Phinney 1991, Tutukov et al. 1992, Tutukov & Yungelson 1993, Lipunov et al. 1995) and is therefore sufficient to explain the observed burst rate which requires an event rate of about 10^{-6} yr^{-1} per galaxy (Narayan et al. 1992). These rates per galaxy are so low that burst repetition in the same region of the sky is practically excluded which is in agreement with the observations (Lamb 1996, Meegan et al. 1995b, Brainerd et al. 1995, Efron & Petrosian 1995). If the merger rate is near the high end of the estimated range, some beaming of the gamma-ray emission might be involved, or the majority of the bursts has to be very dim and escapes detection. Beaming would also lower the energy that must be converted into gamma rays at the source in order to cause the observed fluences.

Since the detected gamma-ray bursts appear to be isotropically distributed and do not visibly trace the large-scale structure of luminous matter in the universe, in particular, are not concentrated towards the supergalactic plane like nearby galaxies, constraints on the distance scale to cosmological bursts can be placed. From the BATSE 3B catalog Quashnock (1996) infers that the comoving distance to the "edge" of the burst distribution is greater than $630\,h^{-1}$ Mpc and the nearest bursts are farther than $40\,h^{-1}$ Mpc (at the 95% confidence level), the median distance to the nearest burst being $170\,h^{-1}$ Mpc (h is the Hubble constant in units of 100 km/s/Mpc). From the absence of anisotropies in supergalactic coordinates, Hartmann et al. (1996) conclude that the minimum sampling distance is $200\,h^{-1}$ Mpc, and Kolatt & Piran (1996) find for their accurate position sub-sample members locations within $600\,h^{-1}$ Mpc. In case of isotropic emission, standard candle non-evolving burst sources at these cosmological distances must release γ-ray energies of the order of $(3...4)\cdot 10^{51}h^{-2}$ erg (Woods & Loeb 1994, Quashnock 1996).

This energy is about 0.1–0.2% of the rest-mass energy of one solar mass or roughly 1% of the gravitational binding energy set free when two 1.5 $M_\odot$ neutron stars merge. A large part of the energy released during the merging, i.e., up to more than 10% of $M_\odot c^2$, is carried away by gravitational waves, the exact value depending on the nuclear equation of state and thus on the compactness of the neutron stars and of the merged object (see Ruffert et al. 1996 and references therein). A similar amount of energy could be radiated away in neutrinos which are abundantly produced when the matter of the coalescing and merging stars is heated up to very high temperatures by tidal forces, friction, and viscous dissipation of kinetic energy in shocks (Eichler et al. 1989, Narayan et al. 1992, Harding 1994). The duration of the neutrino emission, the neutrino luminosity, and the total energy radiated in neutrinos will be determined by the structure and dynamical evolution of the merger, by the thermodynamical conditions in the merging stars, and by the lifetime of the merged object before it collapses into a black hole or before the surrounding material is swallowed by the black hole. Gravitational waves as well as neutrinos from these very distant sources cannot be measured with current experiments, but detectors are planned or built for gravitational waves (LIGO, VIRGO, GEO600; see, e.g., Thorne 1992) and are envisioned for neutrinos (a kilometer-scale neutrino telescope with 1 km^3 of instrumented volume; see Weiler et al. 1994, Halzen & Jaczko 1996, Halzen 1996), which might be lucky to catch the death throes of massive binaries in the not too distant future.

Due to the very high opacity of neutron star matter, high energy photons cannot be emitted by the merging object directly, unless the very outer layers are heated to sufficiently high temperatures. Even if they were radiating with luminosities substantially above the Eddington limit (Duncan et al. 1986), NS-NS or NS-BH mergers at cosmological distances would still be far too faint to be visible from Earth. However, if only a tiny fraction (less than 1%) of the potentially emitted neutrinos and antineutrinos annihilate in the vicinity of the merger (Goodman et al. 1987, Cooperstein et al. 1987) and create a fireball of electron-positron pairs and photons (Cavallo & Rees 1978), an intense outburst of gamma-radiation can be produced with an overall power output exceeding the Eddington luminosity by up to 15 orders of magnitude and energetic enough to account for a cosmological gamma-ray burst (Eichler et al. 1989).

Relativistic expansion of the pair-photon plasma and the final escape of high energy gamma-radiation with the observed non-thermal spectrum (e.g., Band 1993) from an optically thin fireball can only occur if the baryon load of the radiation-pressure ejected shells is sufficiently small, i.e., the contamination with baryons must be below a certain limit (Goodman 1986, Paczyński 1986). If the admixture of baryons is too large, highly relativistic outflow velocities will be impeded through conversion of radiation energy to kinetic energy and the flow will remain optically thick, leading to a degradation of the photons to the UV range (Paczyński 1990, Shemi & Piran 1990). In order to suppress pair production $\gamma + \gamma \to e^+ + e^-$ and to make the fireball optically thin to its own photons, the Lorentz factor Γ of the emitting region must obey $\Gamma \gtrsim 100$ (Fenimore et al. 1993, Mészáros et al. 1993). The bulk Lorentz factor is related with the ratio of total energy to (baryon) rest mass energy: $\Gamma = E_\gamma/(\xi M c^2)$ where ξ is the fraction of the total energy in the fireball that ends up as observed energy in γ-rays, E_γ. Therefore a lower limit for Γ places an upper bound on the amount of baryonic mass M released in the explosive event or being present as ambient gas near the burst source, $M \lesssim 0.6 \cdot 10^{-5}\xi^{-1}(E_\gamma/10^{51}\,\mathrm{erg})\,M_\odot$. Based on the empirical data from the first BATSE catalog (169 bursts), Woods & Loeb (1994) deduce a mean minimum Lorentz factor Γ of about 500, corresponding to an average maximum baryon load of $10^{-5}\xi^{-1}\,M_\odot$ for gamma-ray burst events at cosmological distances. Recent introductory reviews and summaries of the properties of fireballs in the context of cosmological models of gamma-ray bursts were given by Dermer & Weiler (1995), Mészáros (1995), and Piran (1995, 1996).

The limits for the baryon load in the fireball set by observational requirements are very stringent and the baryonic pollution of the pair-photon plasma is a major concern for gamma-ray burst models based on mergers of massive binary stars. In order to obtain $\nu\bar{\nu}$-annihilation in a baryon-poor region around the merger, anisotropies of the merger geometry are considered to be essential (Narayan et al. 1992; Mészáros & Rees 1992a,b; Woosley 1993a; Mochkovitch 1993, 1995a; Hernanz 1994). The hope is that centrifugal forces can keep a region near the rotation axis of the merging NS-NS or NS-BH system relatively baryon free and that the neutrino-driven mass loss from an accretion disk or torus formed after the merging of the binary will leave a "clean" funnel along the axis of symmetry where $\nu\bar{\nu}$-annihilation can create collimated e^+e^- jets expanding relativistically in both axis directions. Also, general relativistic bending of the ν and $\bar{\nu}$ trajectories and $\nu\bar{\nu}$-annihilation inside the innermost stable orbit for massive particles around the accreting black hole have been suggested to be potentially helpful. Secondary processes could lead to the reconversion of baryonic kinetic energy, e.g. by external shock interactions of the expanding fireball in the ambient interstellar medium or pre-ejected gas (Rees & Mészáros 1992; Mészáros & Rees 1992a, 1993; Sari & Piran 1995) or by internal shock interactions of shells having different speeds within the expanding fireball (Narayan et al. 1992, Paczyński & Xu 1994, Rees & Mészáros 1994, Mochkovitch et al. 1995b). Even more complex physics like the upscattering of interstellar photons of a local thermal radiation field by collisions with electrons in the ultrarelativistic wind (Shemi 1994) or highly amplified magnetic fields (Mészáros & Rees 1992a, Usov 1992, Smolsky & Usov 1996) might be important in determining the temporal and spectral structure of the observable gamma-ray burst. In fact, such secondary processes may be crucial to produce the detected very high energy photons with energies of up to more than 1 GeV (Hurley et al. 1994, Teegarden 1995).

In this work we shall not deal with the possibly very complex and complicated processes that are involved in the formation of the finally observable gamma-ray signature. Instead, our interest will be concentrated on the hydrodynamical modelling of the last stages of the coalescence of binary neutron stars employing an elaborate equation of state for neutron star matter with the aim to compute the neutrino emission from the merger. The results of our models will allow us to calculate the efficiency of $\nu\bar{\nu}$-annihilation and the energy deposition in the vicinity of the merging stars. After dozens of papers that suggest and refer to the annihilation of $\nu\bar{\nu}$ pairs from merging compact binaries as the energy source of cosmological gamma-ray bursts, we shall try to put this hypothesis to a quantitative test. We shall investigate the questions whether the neutrino emission from the tidally heated neutron stars just prior to merging (Mészáros & Rees 1992b), during the dynamical phase of the merging or collision (Narayan et al. 1992, Mészáros & Rees 1992b, Dermer & Weiler 1995, Katz & Canel 1995a) or after the merging when a hot accretion disk or torus has possibly formed around a central black hole (Woosley 1993a, Mochkovitch et al. 1993), is sufficiently luminous and lasting to yield the energy required for gamma-ray bursts at cosmological distances. Also, our simulations will provide information about how much mass might remain in an accretion disk or torus and about the thermodynamcial conditions in this disk matter. These aspects might have interesting implications for the possible contributions of NS-NS and NS-BH mergers to the nucleosynthesis of heavy elements.

The paper is organized as follows. In Sect. 2 the computational method and initial conditions for our simulations are described and the hydrodynamical evolution of the merger is shortly summarized from the results given in detail by Ruffert et al. 1996 (Paper I). In Sect. 3 the results for the neutrino emission and thermodynamical evolution of the merger will be presented. Section 4 deals with the neutrino-antineutrino annihilation and contains information about the numerical evaluation (Sect. 4.1), about the numerical results (Sect. 4.2), and about an analytical model which was developed to estimate the neutrino emission and annihilation for an accretion torus around a black hole (Sect. 4.3). In Sect. 5 the results will be discussed concerning their implications for heavy element nucleosynthesis and for gamma-ray bursts, and Sect. 6 contains a summary and conclusions.

2. Computational procedure, initial conditions, and hydrodynamical evolution

In this section we summarize the numerical methods and the treatment of the input physics used for the presented simulations. In addition, we specify the initial conditions by which our different models are distinguished. Also, the results for the dynamical evolution as described in detail in Paper I are shortly reviewed.

2.1. Numerical treatment

The hydrodynamical simulations were done with a code based on the Piecewise Parabolic Method (PPM) developed by Colella & Woodward (1984). The code is basically Newtonian, but contains the terms necessary to describe gravitational wave emission and the corresponding back-reaction on the hydrodynamical flow (Blanchet et al. 1990). The modifications that follow from the gravitational potential are implemented as source terms in the PPM algorithm. The necessary spatial derivatives are evaluated as standard centered differences on the grid.

In order to describe the thermodynamics of the neutron star matter, we use the equation of state (EOS) of Lattimer & Swesty (1991) in a tabular form. The inversion for the temperature is done with a bisection iteration. Energy loss and changes of the electron abundance due to the emission of neutrinos and antineutrinos are taken into account by an elaborate "neutrino leakage scheme". The energy source terms contain the production of all types of neutrino pairs by thermal processes and of electron neutrinos and antineutrinos also by lepton captures onto baryons. The latter reactions act as sources or sinks of lepton number, too, and are included as source term in a continuity equation for the electron lepton number. When the neutron star matter is optically thin to neutrinos, the neutrino source terms are directly calculated from the reaction rates, while in case of optically thick conditions lepton number and energy are released on the corresponding neutrino diffusion time scales. The transition between both regimes is done by a smooth interpolation. Matter is rendered optically thick to neutrinos due to the main opacity producing reactions which are neutrino-nucleon scattering and absorption of neutrinos onto baryons.

More detailed information about the employed numerical procedures can be found in Paper I, in particular about the implementation of the gravitational wave radiation and back-reaction terms and the treatment of the neutrino lepton number and energy loss terms in the hydrodynamical code.

2.2. Initial conditions

We start our simulations with two identical Newtonian neutron stars with a baryonic mass of about 1.63 $M_\odot$ and a radius of 15 km which are placed at a center-to-center distance of 42 km on a grid of 82 km side length. With the employed EOS of Lattimer & Swesty (1991), this baryonic mass corresponds to a (general relativistic) gravitational mass of approximately 1.5 $M_\odot$ for a cool star with a radius as obtained from the general relativistic stellar structure equations of 11.2 km. Having a compressibility modulus of bulk nuclear matter of $K = 180$ MeV (which is the "softest" of the three available cases), the Lattimer & Swesty EOS may overestimate the stiffness of supranuclear matter, in particular, since in its present form it neglects the possible occurrence of new hadronic states besides the neutron and proton at very high densities. For a softer supranuclear EOS, neutron stars would become more compact and their gravitational binding energy larger so that a baryonic mass of 1.63 $M_\odot$ would more likely correspond to a gravitational mass between 1.4 and 1.45 $M_\odot$.

The distributions of density ρ and electron fraction Y_e are taken from a one-dimensional model of a cold, deleptonized neutron star in hydrostatic equilibrium. For numerical reasons the surroundings of the neutron stars cannot be assumed to be evacuated. The density of the ambient medium was set to 10^9 g/cm^3, more than five orders of magnitude smaller than the central densities of the stars. The internal energy density and electron fraction of this gas were taken to be equal to the values in the neutron stars at a density of 10^9 g/cm^3. In order to ensure sufficiently good numerical resolution, we artificially softened the extremely steep density decline towards the neutron star surfaces by not allowing for a density change of more than two orders of magnitude from zone to zone. From this prescription we obtain a thickness of the neutron star surface layers of about 3 zones.

Table 1. Parameters and some computed quantities for all models. N is the number of grid zones per dimension in the orbital plane, S defines the direction of the spins of the neutron stars relative to the direction of the orbital angular momentum, and $k_\mathrm{B}T_\mathrm{ex}$ gives the maximum temperature (in energy units) reached on the grid during the simulation of a model. L_{ν_e} is the electron neutrino luminosity after approaching a saturation level at about 8 ms, $L_{\bar\nu_e}$ is the corresponding electron antineutrino luminosity, and L_{ν_x} the luminosity of each individual species of ν_μ, $\bar\nu_\mu$, ν_τ, $\bar\nu_\tau$. L_ν gives the total neutrino luminosity after a quasi-stationary state has been reached at $t \gtrsim$ 6–8 ms and $\dot E_{\nu\bar\nu}$ denotes the integral rate of energy deposition by neutrino-antineutrino annihilation at that time

Model	N	S	$k_\mathrm{B}T_\mathrm{ex}$ MeV	L_{ν_e} 10^{53}erg/s	$L_{\bar\nu_e}$ 10^{53}erg/s	L_{ν_x} 10^{53}erg/s	L_ν 10^{53}erg/s	$\dot E_{\nu\bar\nu}$ 10^{50}erg/s
A64	64	0	40	0.13	0.58	0.11	1.15	2.1
B64	64	+1	30	0.18	0.55	0.09	1.09	3.0
C64	64	−1	>50	0.15	0.67	0.10	1.22	3.6
A128	128	0	39	0.16	0.43	0.06	0.83	—

The orbital velocities of the coalescing neutron stars were prescribed according to the motion of point masses spiralling towards each other due to the emission of gravitational waves. The tangential velocities of the neutron star centers were set equal to the Kepler velocities on circular orbits and radial velocity components were attributed as calculated from the quadrupole formula. In addition to the orbital angular momentum, spins around their respective centers were added to the neutron stars. The assumed spins and spin directions were varied between the calculated models. Table 1 lists the distinguishing model parameters, the number N of grid zones per spatial dimension (in the orbital plane) and the spin parameter S. The neutron stars in models A64 and A128 did not have any additional spins ($S = 0$), in model B64 the neutron star spins were parallel to the orbital angular momentum vector ($S = +1$), in model C64 the spins were in the opposite direction ($S = -1$). In both models B64 and C64, the angular velocities of the rigid neutron star rotation and of the orbital motion were chosen to be equal. Model A128 had the same initial setup as model A64 but had twice the number of grid zones per spatial dimension and thus served as a check for the sufficiency of the numerical resolution of the computations with 64^3 zones.

The rotational state of the neutron stars is determined by the action of viscosity. If the dynamic viscosity of neutron star matter were large enough, tidal forces could lead to tidal locking of the two stars and thus spin-up during inspiral. Kochanek (1992), Bildsten & Cutler (1992), and Lai (1994), however, showed that microscopic shear and bulk viscosities are probably orders of magnitude too small to achieve corotation. Moreover, they argued that for the same reason it is extremely unlikely that the stars are heated up to more than about 10^8 K by tidal interaction prior to merging. In this sense, models A64 and A128 can be considered as reference case for two non-corotating neutron stars, while model B64 represents the case of rigid-body like rotation of the two stars, and model C64 the case where the spin directions of both stars were inverted.

Since in the case of degenerate matter the temperature is extremely sensitive to small variations of the internal energy, e.g. caused by small numerical errors, we did not start our simulations with cold ($T = 0$) or "cool" ($T \lesssim 10^8$ K) neutron stars as suggested by the investigations of Kochanek (1992), Bildsten & Cutler (1992), and Lai (1994). Instead, we constructed initial temperature distributions inside the neutron stars by assuming thermal energy densities of about 3% of the degeneracy energy density for a given density ρ and electron fraction Y_e. The corresponding central temperature was around 7 MeV and the average temperature was a few MeV and thus of the order of the estimates obtained by Mészáros & Rees (1992b) for the phase just prior to the merging. Locally, these initial temperatures were much smaller than the temperatures produced by the compression and dissipative heating during coalescence (see Table 1 for the maximum temperatures). However, they are orders of magnitude larger than can be achieved by tidal dissipation with plausible values for the microscopic viscosity of neutron star matter. Even under the most extreme assumptions for viscous shear heating, the viscosity of neutron star matter turns out to be at least four orders of magnitude too small (see Janka & Ruffert 1996).

Models A64, B64, and C64 were computed on a Cray-YMP 4/64 where they needed about 16 MWords of main memory and took approximately 40 CPU-hours each. For the better resolved model A128 we employed a grid with $128 \times 128 \times 64$ zones instead of the $64 \times 64 \times 32$ grid of models A64, B64, and C64. Note that in the direction orthogonal to the orbital plane only half the number of grid zones was used but the spatial resolution was the same as in the orbital plane. Model A128 was run on a Cray-EL98 4/256 and required about 22 MWords of memory and 1700 CPU-hours.

2.3. Hydrodynamical evolution

The hydrodynamical evolution and corresponding gravitational wave emission were detailed in Paper I. Again, we only summarize the most essential aspects here.

The three-dimensional hydrodynamical simulations were started at a center-to-center distance of the two neutron stars of 2.8 neutron star radii. This was only slightly larger than the separation where the configurations become dynamically unstable which is at a distance of approximately 2.6 neutron star radii. Gravitational wave emission leads to the decay of the binary orbit, and already after about one quarter of a revolution, approximately 0.6 ms after the start of the computations, the neutron star surfaces touch because of the tidal deformation and stretching of the stars.

When the two stars begin to plunge into each other, compression and the shearing motion of the touching surfaces cause dissipation of kinetic energy and lead to a strong increase of the temperature. From initial values of a few MeV, the gas heats up to peak temperatures of several ten MeV. In case of model C64, a temperature of nearly 50 MeV is reached about 1 ms after the stars have started to merge. After one compact, massive body has formed from most of the mass of the neutron stars about 3 ms later, more than 50 MeV are found in two distinct, extremely hot off-center regions.

At the time of coalescence and shortly afterwards, spiral-arm or wing-like extensions are formed from material spun off the outward directed sides of the neutron stars by tidal and centrifugal forces. Due to the retained angular momentum, the central body performs large-amplitude swinging motions and violent oscillations. This wobbling of the central body of the merger creates strong pressure waves and small shocks that heat the exterior layers and lead to the dispersion of the spiral arms into a vertically extended "ring" or thick toroidal disk of gas that surrounds the massive central object. While the mass of the compact body is larger than 3 $M_\odot$ and its mean density above $10^{14}\ \mathrm{g/cm^3}$, the surrounding cloud contains only 0.1–0.2 $M_\odot$ and is more dilute with an average density of about $10^{12}\ \mathrm{g/cm^3}$.

The central body is too massive to be stabilized by gas pressure for essentially all currently discussed equations of state of nuclear and supranuclear matter. Moreover, it can be argued (see Paper I) that its angular momentum is not large enough to provide rotational support. Therefore, we expect that in a fully general relativistic simulation, the central object will collapse into a black hole on a time scale of only a few milliseconds after the neutron stars have merged. Dependent on the total angular momentum corresponding to the initial setup of the neutron star spins, some of the material in the outer regions of the disk obtains enough angular momentum (e.g., by momentum transfer via pressure waves) to flow across the boundary of the computational grid at a distance of about 40 km from the center. In model B64 which has the largest total angular momentum because of the assumed solid-body type rotation, 0.1–0.15 $M_\odot$ are able to leave the grid between 2 ms and 4 ms after the start of the simulation. However, at most a few times $10^{-4}\ M_\odot$ of this material have a total energy that might allow them to escape from the gravitational field of the merger. In model C64 the anti-spin setup leads to violent oscillations of the merged body which create a very extended and periodically contracting and reexpanding disk. In this model nearly $0.1\ M_\odot$ are lost across the outer grid boundaries even during the later stages of the simulation ($t \gtrsim 5$ ms).

While by far the major fraction of the merger mass ($\gtrsim 3\ M_\odot$) will be swallowed up by the forming black hole almost immediately on a dynamical time scale, some matter with sufficiently high specific angular momentum might be able to remain in a disk around the slowly rotating black hole. Estimates show (Paper I) that with the typical rotation velocities obtained in our models, this matter must orbit around the central body at radii of at least between about 40 km and 100 km. This means that only matter that has been able to leave the computational grid used in our simulations has a chance to end up in a toroidal disk around the black hole. From these arguments we conclude that such a possible disk might contain a mass of at most 0.1–0.15 $M_\odot$.

3. Neutrino emission and thermodynamical evolution

3.1. Neutrino emission

The local energy and lepton number losses due to neutrino emission are included via source terms in our code as described in the appendix of Paper I. We treated the neutrino effects in terms of an elaborate leakage scheme that was calibrated by comparison with results from diffusion calculations in one-dimensional situations. By adding up the local source terms over the whole computational grid, one obtains the neutrino luminosities of all individual neutrino types, the sum of which gives the total neutrino luminosity. In the same way number fluxes of electron neutrinos (ν_e), electron antineutrinos ($\bar\nu_e$), and heavy-lepton neutrinos (ν_μ, $\bar\nu_\mu$, ν_τ, and $\bar\nu_\tau$, which will be referred to as ν_x in the following) can be calculated. The mean energies of the emitted neutrinos result from the ratios of neutrino luminosities to neutrino number fluxes.

Figures 1–4 display the results for the neutrino fluxes and mean energies of the emitted neutrinos for our models A64, B64, C64, and A128. In Fig. 1 one can see that the total neutrino luminosities start to increase above $\sim 10^{52}\,\mathrm{erg/s}$ at about 2.5–3.5 ms after the start of the simulations. This is about the time when the spiral arm structures become dispersed into a spread-out cloud of material that surrounds the merger and is heated by the interaction with compression waves. At the same time the temperatures in the interior of the massive central body reach their peak values. Since the neutrino luminosities are by far dominated by the contributions from the disk emission (see below), the heating of the cloud and torus material is reflected in a continuous increase of the neutrino fluxes. Also, the dynamical expansions and contractions caused by the oscillations and wobbling of the central body impose fluctuations on the light curves. The periodic expansions and contractions have particularly large amplitudes in model C64 because of the anti-spin setup of the neutron star rotations which leads to very strong internal shearing and turbulent motions after merging as well as to higher temperatures than in the other models (see Table 1). The light curve fluctuations in model C64 are as large as 25–30% of the average luminosity and proceed with a period of 0.5–1 ms which is about the dynamical time scale of the merger. When the oscillating central body enters an expansion phase, very hot matter that is located in a shell around the central core of the merger, is swept to larger radii. In course of the expansion the neutrino optical depth decreases and the very hot material releases enhanced neutrino fluxes. The neutrino outburst is terminated, when the surface-near matter has cooled by adiabatic expansion or when re-contraction sets in and the neutrino optical depth increases again. At times later than about 6–8 ms quasi-stationary values of the fluxes are reached which are between about $8 \cdot 10^{52}\,\mathrm{erg/s}$ in case of model A128 and about $1.3 \cdot 10^{53}\,\mathrm{erg/s}$ for C64.

Figure 2 shows that the energy lost in gravitational waves during the merging is about two orders of magnitude larger than the energy radiated away in neutrinos during the simulated period of approximately 10 ms. While the gravitational wave luminosity peaks around the time when the dynamical instability of the orbit sets in and the two neutron stars start to interact dynamically and fuse into a single object (t between 0.5 ms and 1.5 ms), the energy emitted in neutrinos becomes sizable only after the extended toroidal cloud of matter has formed around the merged stars.

The heated torus or "disk" consists of decompressed neutron star matter with an initially very low electron number fraction Y_e between about 0.01 and 0.04. The neutrino emission of the disk is therefore clearly dominated by the loss of electron antineutrinos which are primarily produced in the process $e^+ + n \to p + \bar\nu_e$, because positrons are rather abundant in the hot and only moderately degenerate, neutron-rich matter (see Sect. 3.2). In Fig. 3 one sees that the $\bar\nu_e$ luminosity $L_{\bar\nu_e}$ is a factor 3–4.5 larger than L_{ν_e} and between $5.5 \cdot 10^{52}\,\mathrm{erg/s}$ for model B64 and about $6.7 \cdot 10^{52}\,\mathrm{erg/s}$ for C64 when quasi-stationary conditions have been established after about 6 ms from the start of the simulations (Table 1). The sum of all heavy-lepton neutrino fluxes which is four times the individual luminosities of ν_μ, $\bar\nu_\mu$, ν_τ or $\bar\nu_\tau$, is around $4 \cdot 10^{52}\,\mathrm{erg/s}$. The better resolved model A128 yields slightly smaller values for all luminosities than A64 (Table 1).

The mean energies of the emitted neutrinos are displayed in Fig. 4 for models A64, B64, and C64. The differences between the different models are smaller than in case of the neutrino lu-

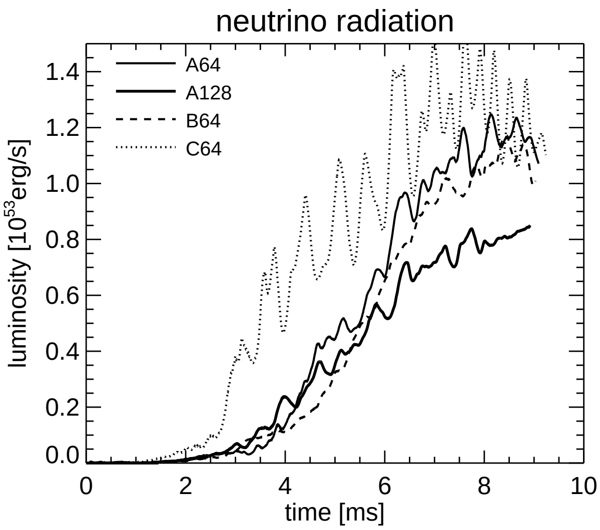

Fig. 1. Total neutrino luminosities as functions of time for all four models

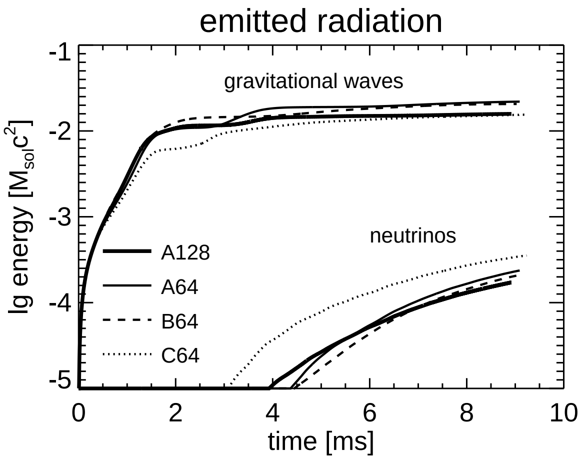

Fig. 2. Comparison of the cumulative energies emitted in gravitational waves and in neutrinos as functions of time for all four models

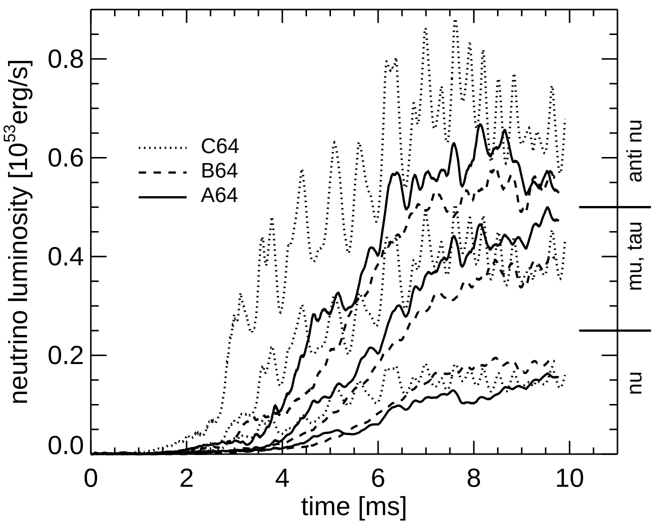

Fig. 3. Luminosities of individual neutrino types (ν_e, $\bar{\nu}_e$, and the sum of all ν_x) as functions of time for the three models A64, B64, and C64

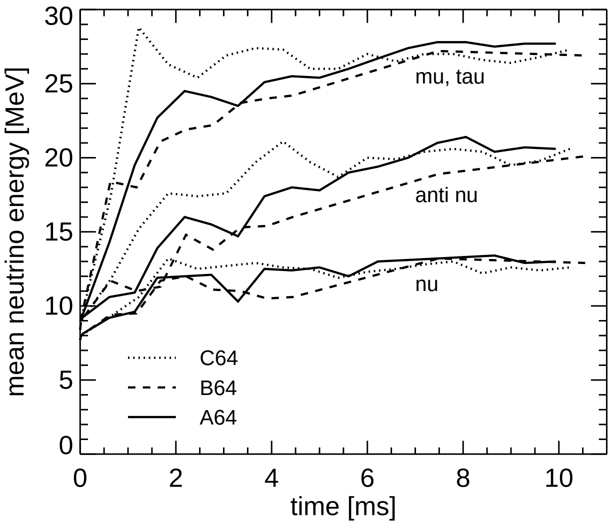

Fig. 4. Average energies of emitted neutrinos ν_e, $\bar{\nu}_e$, and ν_x as functions of time for the three models A64, B64, and C64

minosities. This means that the effective temperatures in the neutrinospheric regions are very similar in all models. Electron neutrinos are emitted with an average energy of 12–13 MeV, electron antineutrinos have 19–21 MeV, and heavy lepton neutrinos leave the merger with mean energies of 26–28 MeV during the stationary phase. Except for the dominance of $L_{\bar{\nu}_e}$ relative to L_{ν_e}, both the mean neutrino energies and the neutrino luminosities are in good overall agreement with typical numbers obtained in stellar core collapse and supernova simulations at a stage some time after the prompt ν_e burst has been emitted and after the collapsed stellar core has heated up along with the post-shock settling (see, e.g., Mayle et al. 1987, Myra & Burrows 1990, Bruenn 1993, Bruenn et al. 1995).

Just like the neutrino emission from the less opaque, hot mantle region of the protoneutron star dominates the supernova neutrino fluxes for several ten to some hundred milliseconds after core bounce, more than 90% of the neutrino emission of the merger comes from the extended, hot torus and only a minor fraction of less than 10% originates from the very opaque and dense central core of the merged object. Figures 5,

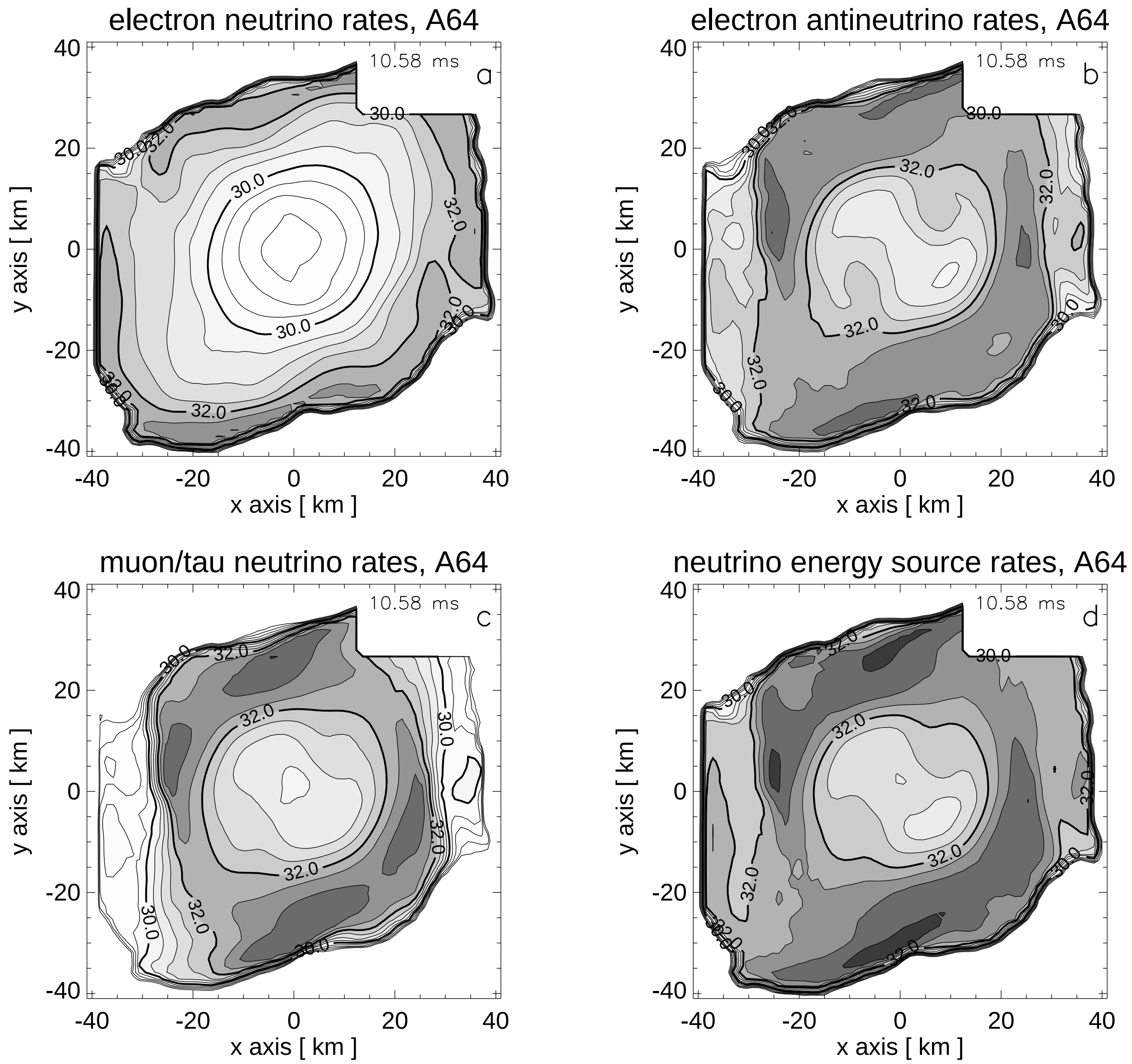

Fig. 5. Energy emission rates (in erg/cm^3/s) of electron neutrinos (panel **a**), electron antineutrinos (panel **b**), the sum of all heavy-lepton neutrinos (panel **c**), and the total neutrino energy loss rate in the orbital plane of model A64 at the end of the simulation (time in the top right corner of the panels). The contours are logarithmically spaced in intervals of 0.5 dex, bold contours are labeled with their respective values. The grey shading emphasizes the emission levels, dark grey corresponding to the strongest energy loss by neutrino emission

6, 8, and 9 display the local emission rates of ν_e, $\bar{\nu}_e$, the sum of ν_x, and the sum of all neutrino types in the orbital plane for models A64, A128, B64, and C64, respectively, at a time when quasi-stationary conditions have been established. Figures 7 and 10 give the corresponding information in two orthogonal cut planes vertical to the equatorial plane for the representative models A128 and C64. One can clearly see that the surface-near regions, in particular the toroidal cloud of matter surrounding the central, compact body, emits neutrinos at much higher rates.

Using the values from these figures, one can estimate the relative importance of core and disk emission. The dense core regions ($\rho \gtrsim 10^{13}\,\mathrm{g/cm^3}$) inside a radius of $R_{\mathrm{c}} \approx 20$ km lose neutrino energy with a typical rate of $Q_\varepsilon \approx 10^{32}\,\mathrm{erg/cm^3/s}$ and account for a luminosity of about $L_{\nu,\mathrm{c}} \approx (4\pi/3)R_{\mathrm{c}}^3 Q_\varepsilon \approx 3.4\cdot 10^{51}\,\mathrm{erg/s}$, while the emission from the surrounding torus-shaped disk region with outer radius $R_{\mathrm{d}} \approx 40$ km, height $2h \approx 40$ km, and typical total neutrino energy loss rate $Q_\varepsilon \approx 5\cdot 10^{32}\,\mathrm{erg/cm^3/s}$ emits a luminosity of roughly $L_{\nu,\mathrm{d}} \approx$

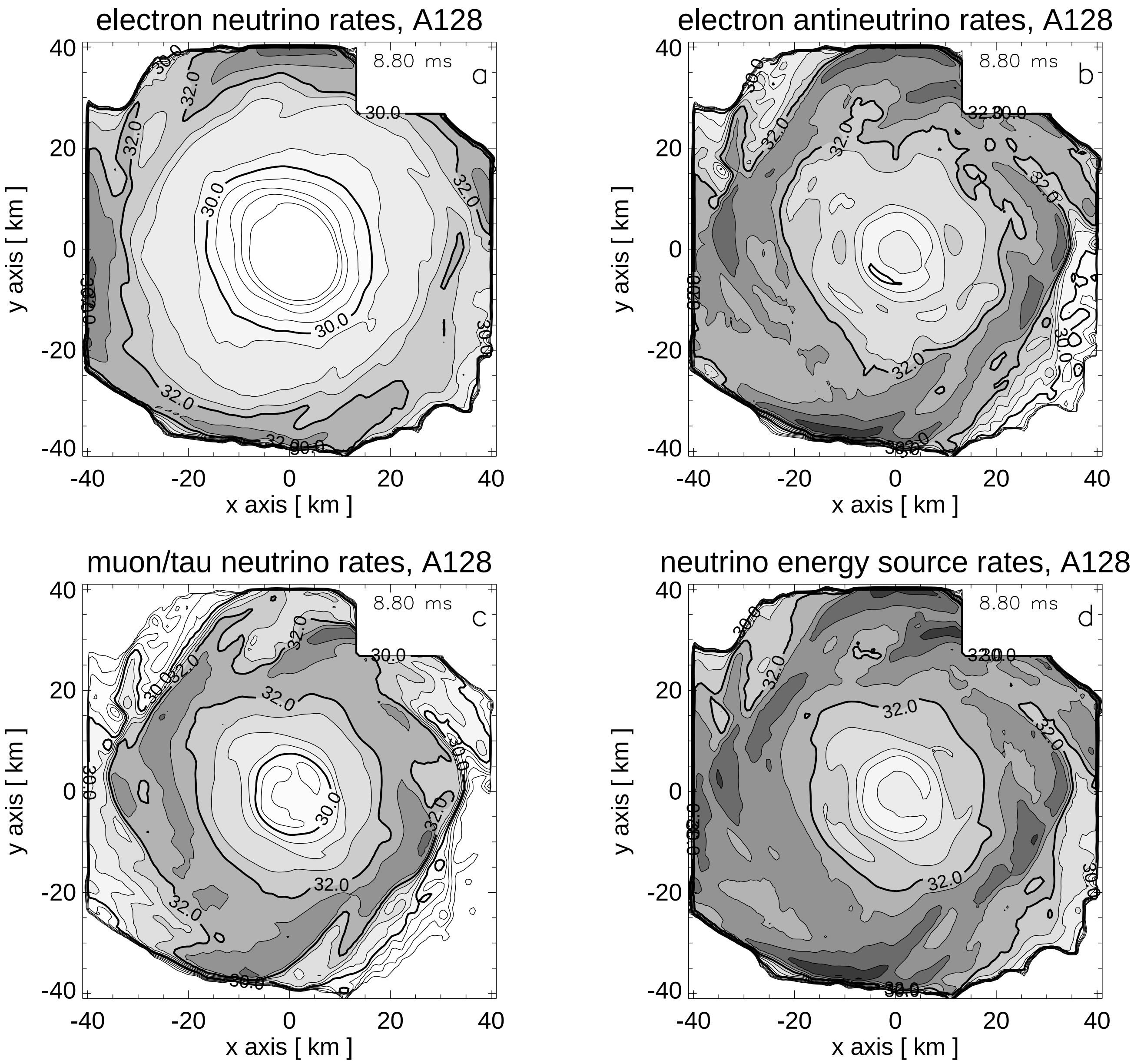

Fig. 6. Same as Fig. 5 but for model A128 at time $t = 8.80$ ms. The higher resolution of this simulation allows more fine structure to be visible

$(2\pi R_{\rm d}^2 h - 4\pi R_{\rm c}^3/3)Q_\varepsilon \approx 8.4 \cdot 10^{52}$ erg/s. The sum of $L_{\nu,\rm c}$ and $L_{\nu,\rm d}$ is of the size of the results displayed in Fig. 1.

Figures 5–10 also demonstrate that the disk emits $\bar\nu_e$ fluxes that are larger than the ν_e fluxes. Electron neutrinos are most strongly emitted from surface-near regions where the optical depth to ν_e by absorption on neutrons ($\nu_e + n \to p + e^-$) in the neutron-rich matter is smallest. In contrast, the production of electron antineutrinos by positron captures on neutrons and of heavy-lepton neutrinos via electron-positron pair annihilation ($e^- + e^+ \to \nu + \bar\nu$) requires the presence of large numbers of positrons and therefore occurs predominantly in those parts of the disk which have been heated most strongly and have a low electron degeneracy. Since $\bar\nu_e$ are absorbed on the less abundant protons in the inverse β^+ process and the opacity to ν_x is primarily caused by neutrino-nucleon scatterings only, electron antineutrinos and heavy-lepton neutrinos can escape on average from deeper and hotter layers than electron neutrinos (see Figs. 5–10). This explains the higher mean energies of the emitted $\bar\nu_e$ and ν_x.

As expected from the very similar neutrino luminosities and nearly equal mean energies of emitted neutrinos, the neutrino emission maps do not reveal major differences between the models A64, B64, and C64. Most neutrino emission comes from the disk region where the neutrino optical depths are lower, and in Figs. 5, 8, and 9 one can clearly recognize the high-density, very opaque inner part of the core of the merger

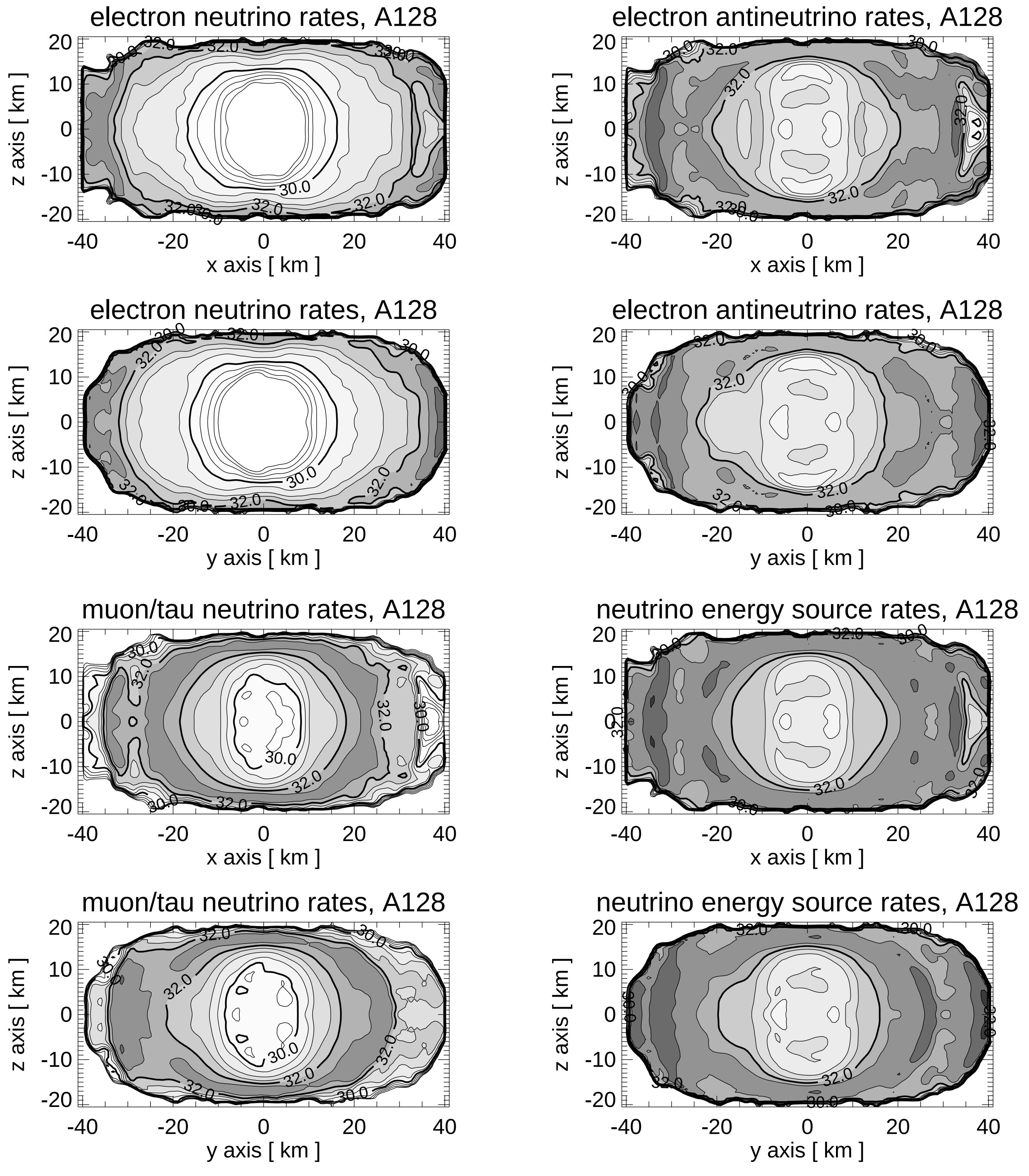

Fig. 7. Energy loss rates by neutrino emission in two orthogonal planes vertical to the orbital plane for model A128 at time $t = 8.80$ ms. The displayed information is the same as in Fig. 5

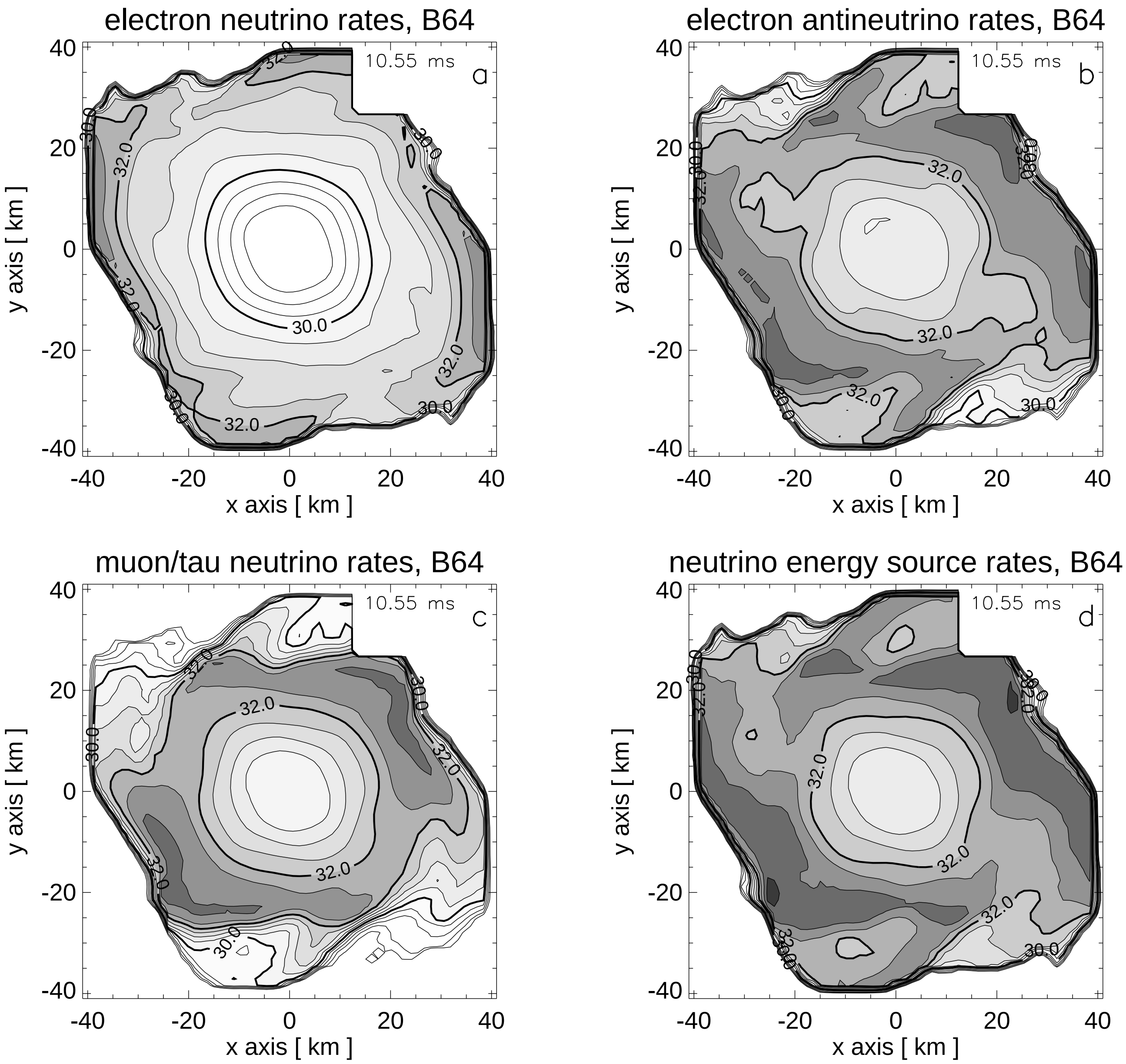

Fig. 8. Same as Fig. 5 but for model B64 at time $t = 10.55$ ms

from its roughly two orders of magnitude smaller energy loss rates. The cuts perpendicular to the orbital plane (see Fig. 10) show the ring-like main emission region that surrounds the central core and has a banana- or dumb-bell shaped cross section. Model A128 has significantly more fine structure but the overall features and characteristics of the neutrino emission do not change with the much better numerical resolution of this simulation.

3.2. Thermodynamics and composition

Figure 11 displays contour levels in the temperature-density plane of the electron neutrino chemical potential (measured in MeV) for an electron fraction of $Y_e = 0.046$. In Fig. 12 the contours corresponding to vanishing electron neutrino chemical potential $\mu_{\nu_e} = 0$ are plotted for different values of Y_e. Figures 11 and 12 provide information about how chemical equilibrium is shifted according to the equation of state of Lattimer & Swesty (1991) when neutron star matter changes its temperature-density state.

Cold neutron star matter at neutrinoless β-equilibrium is in a state with $\mu_{\nu_e} = 0$. When such gas of the outermost ~ 0.1–$0.2\,M_\odot$ of the neutron star with density $\rho \lesssim 10^{14}\ \mathrm{g/cm^3}$ and electron fraction $Y_e \lesssim 0.025$ (see Fig. 2 in Paper I) is expanded and heated while the lepton fraction $Y_{\rm lep} = Y_e + Y_{\nu_e} \approx Y_e$ stays roughly constant as it is the case for a fast change where neu-

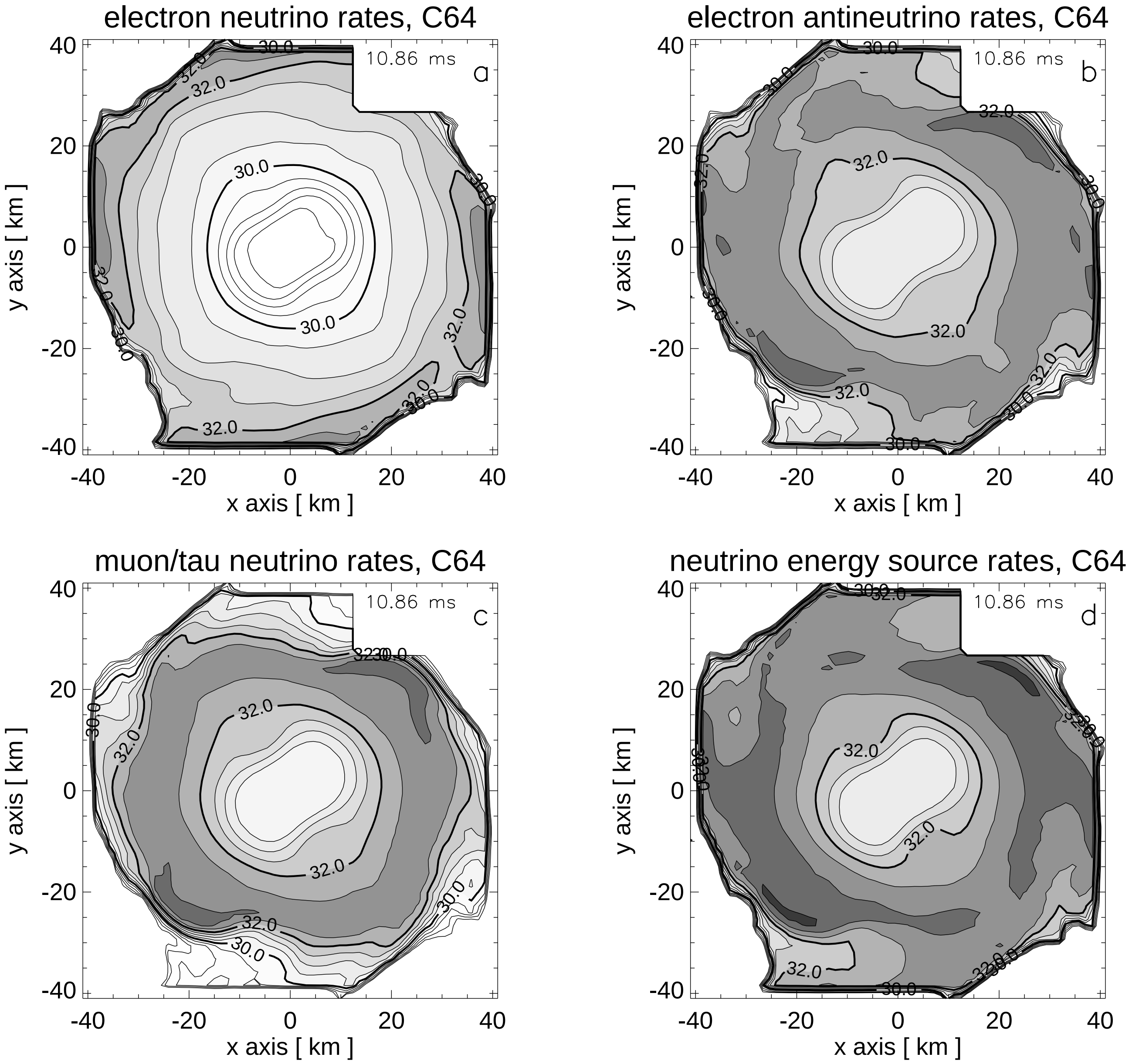

Fig. 9. Same as Fig. 5 but for model C64 at time $t = 10.86$ ms

trino losses are too slow to compete, the β-equilibrium is shifted into the region of negative μ_{ν_e} values. This usually implies that the electron degeneracy of the matter is drastically decreased, too, because the electron chemical potential $\mu_e = \mu_{\nu_e} + \mu_n - \mu_p$ also drops when μ_{ν_e} attains negative values. For hot gas (i.e., gas at conditions lying above the nose-like feature of the curves in Figs. 11 and 12) the state with $\mu_{\nu_e} = 0$ corresponds to a higher value of Y_e which is seen in Fig. 12 by moving along lines parallel to the ordinate. On the lepton-number loss time scale associated with neutrino emission, the gas will tend to evolve again towards the β-equilibrium with $\mu_{\nu_e} = 0$ by an enhanced production and emission of $\bar{\nu}_e$ relative to ν_e. Notice that from Figs. 11 and 12 one infers that the same arguments are true for the case that neutron star matter with densities above $\rho \approx 10^{14}\,\mathrm{g/cm^3}$ is strongly compressed. From the properties of the high-density equation of state we therefore deduce that during the coalescence of neutron star binaries the hot gas in the compact, compressed core region of the merger as well as the heated, decompressed disk matter will radiate $\bar{\nu}_e$ more copiously than ν_e.

This explains the relative sizes of electron neutrino and antineutrino luminosities as discussed in Sect. 3.1. Driven by this imbalance of the emission of ν_e and $\bar{\nu}_e$, the initially very neutron-rich matter ($Y_e \lesssim 0.095$ everywhere in the neutron star, see Fig. 2 in Paper I) gains electron lepton number and becomes more proton-rich again. Figure 13 shows this evolution

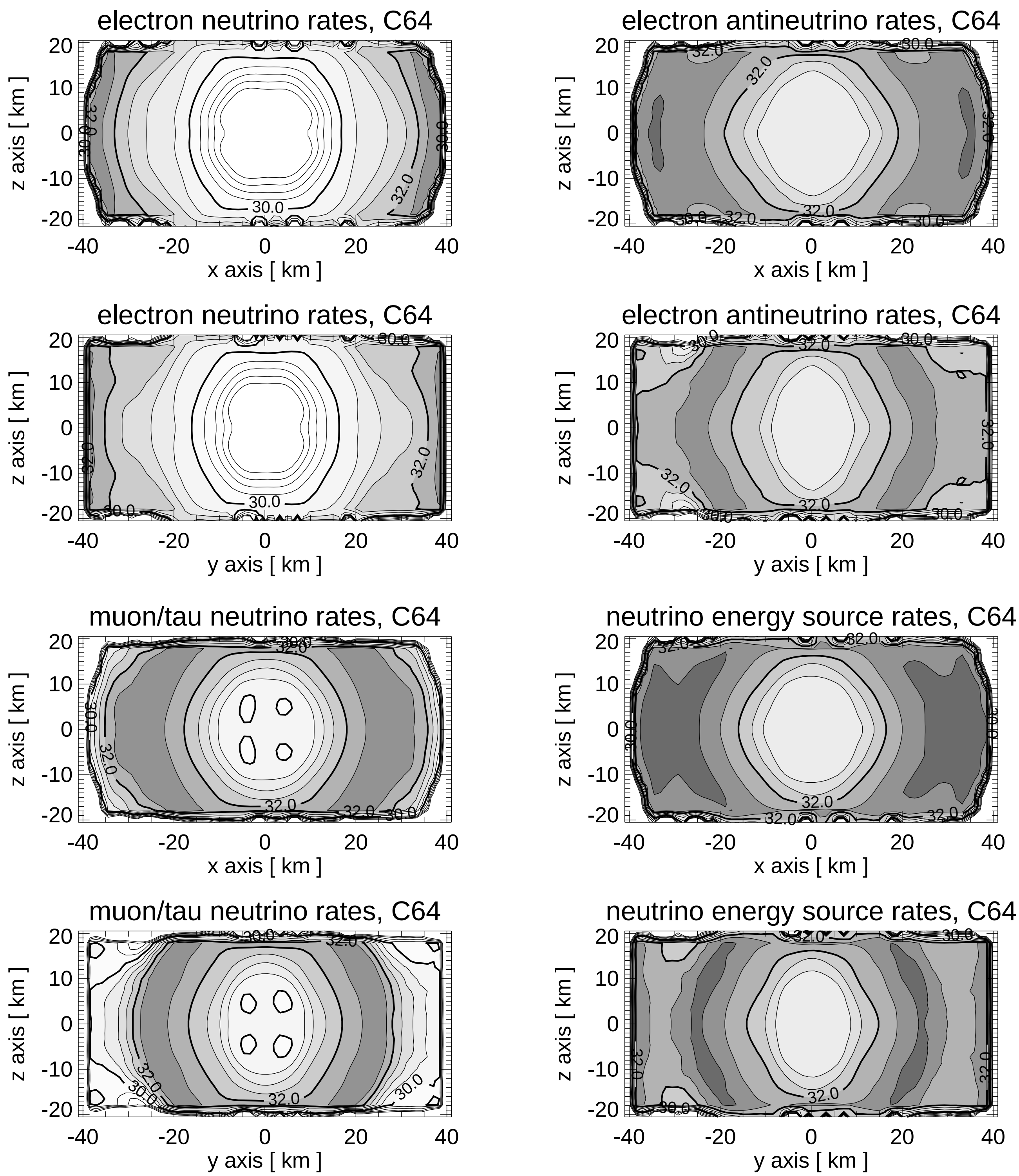

Fig. 10. Same as Fig. 7 but for model C64 at time $t = 10.86$ ms

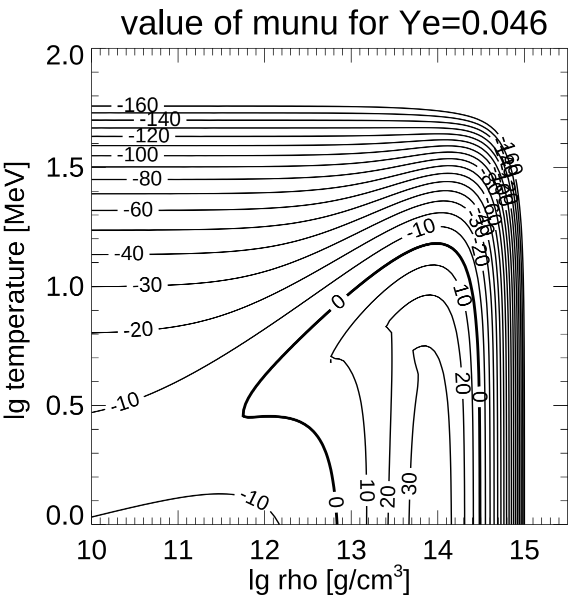

Fig. 11. Contours of the neutrino chemical potential (measured in MeV) in the temperature-density plane for fixed electron fraction Y_e. The contours are spaced with increments of 10 and are labeled with their respective values

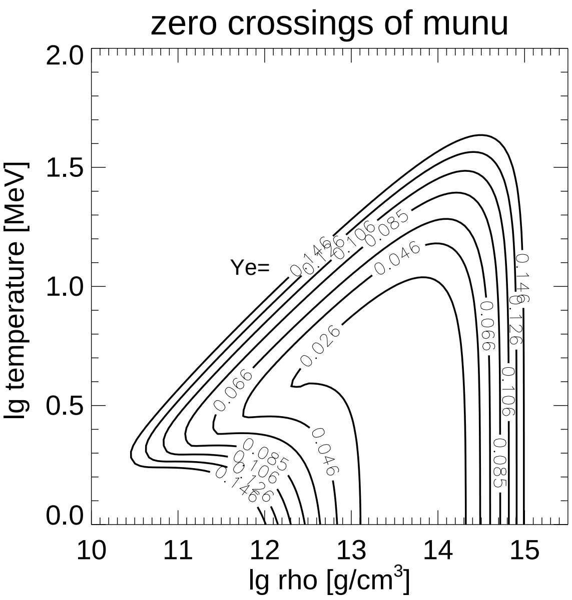

Fig. 12. Contours of vanishing neutrino chemical potential ($\mu_\nu = 0$) in the temperature-density plane for different values of the electron fraction Y_e as indicated by the line labels

for model A128 from the start of the simulation until its end at 8.80 ms. The snapshots of the Y_e distribution in the orbital plane visualize how, as a consequence of the rapid neutrino loss from the disk region, Y_e in this region climbs from initial values of 0.02–0.06 to values of more than 0.18 in some parts. In the core region the neutrino emission proceeds much more slowly so that Y_e changes only slightly during the simulated time. If we continued our computations for a long enough time to see the matter cooling again by neutrino losses (provided the configuration is stable for a sufficiently long period), this process of Y_e increase would again be inverted and the gas would evolve towards the cold, deleptonized, very neutron-rich state again.

Figure 14 displays the final situations ($t \approx$ 10–11 ms) in the models A64, B64, and C64 to be compared with panel **f** of Fig. 13. As in case of the neutrino emission, one notices very similar properties of all four models. In model A64 the peak Y_e values in the disk region are as high as 0.22. Note that in all four models very neutron-rich matter is swept off the grid, a tiny fraction of which might potentially become unbound (see Sect. 2.3 and Paper I). It is also interesting to see the still very elongated and deformed neutron-rich inner region of models A64 and B64 which indicates ongoing strong dynamical and pulsational activity of the massive core. This is not so pronounced in model C64 where the anti-spin setup of the initial model has caused the dissipation of a large fraction of the rotational energy during the coalescence of the neutron stars. Model A128 has also a much more circular core region because, as described in Paper I, the better resolution allows for a much more fine-granular flow pattern which contains a large fraction of the initial vorticity and kinetic energy in small vortex structures.

Figure 15 presents a collection of plots of parameters that give information about the thermodynamical state in the orbital plane of model A128 and about the nuclear composition of the gas at the end of the simulation. Panels **a** and **b** show the electron degeneracy parameter $\eta_e = \mu_e/(k_{\rm B}T)$ ($k_{\rm B}$ is the Boltzmann constant, μ_e the electron chemical potential) and the electron neutrino degeneracy parameter $\eta_{\nu_e} = \mu_{\nu_e}/(k_{\rm B}T)$, respectively. Concordant with the discussion above, the β-equilibrium conditions in the whole star are characterized by $\eta_{\nu_e} \lesssim 0$ (panel **b**). In the core values between -3 and -6 can be found, while in the disk moderately negative values are present (around -1) and in some regions the medium has evolved back to a state close to $\eta_{\nu_e} \approx 0$. Comparison with panels **a** and **b** of Fig. 6 shows that in these regions the emission rates of ν_e and $\bar\nu_e$ are already very similar again whereas the production of electron antineutrinos is clearly dominant in those parts of the disk with the most negative values of η_{ν_e}. The electron degeneracy is moderate ($\eta_e \approx$ 2–3) in the disk but climbs to numbers around $\eta_e \approx 25$ near the center.

The temperature $k_{\rm B}T$ and entropy are displayed in panels **c** and **d**, respectively, of Fig. 15. Detailed information about the evolution of the temperature in all models was given in Paper I (Figs. 4–7, 14–17, and 20, 21). At the end of the simulation model A128 has the highest temperatures of $k_{\rm B}T \approx 30$ MeV in hot spots located in a shell around the central high-density core where $k_{\rm B}T \approx 10$ MeV. The disk has been heated up to $k_{\rm B}T \approx 10$ MeV in regions of density $\rho \approx 10^{12}$–$10^{13}\,{\rm g/cm^3}$,

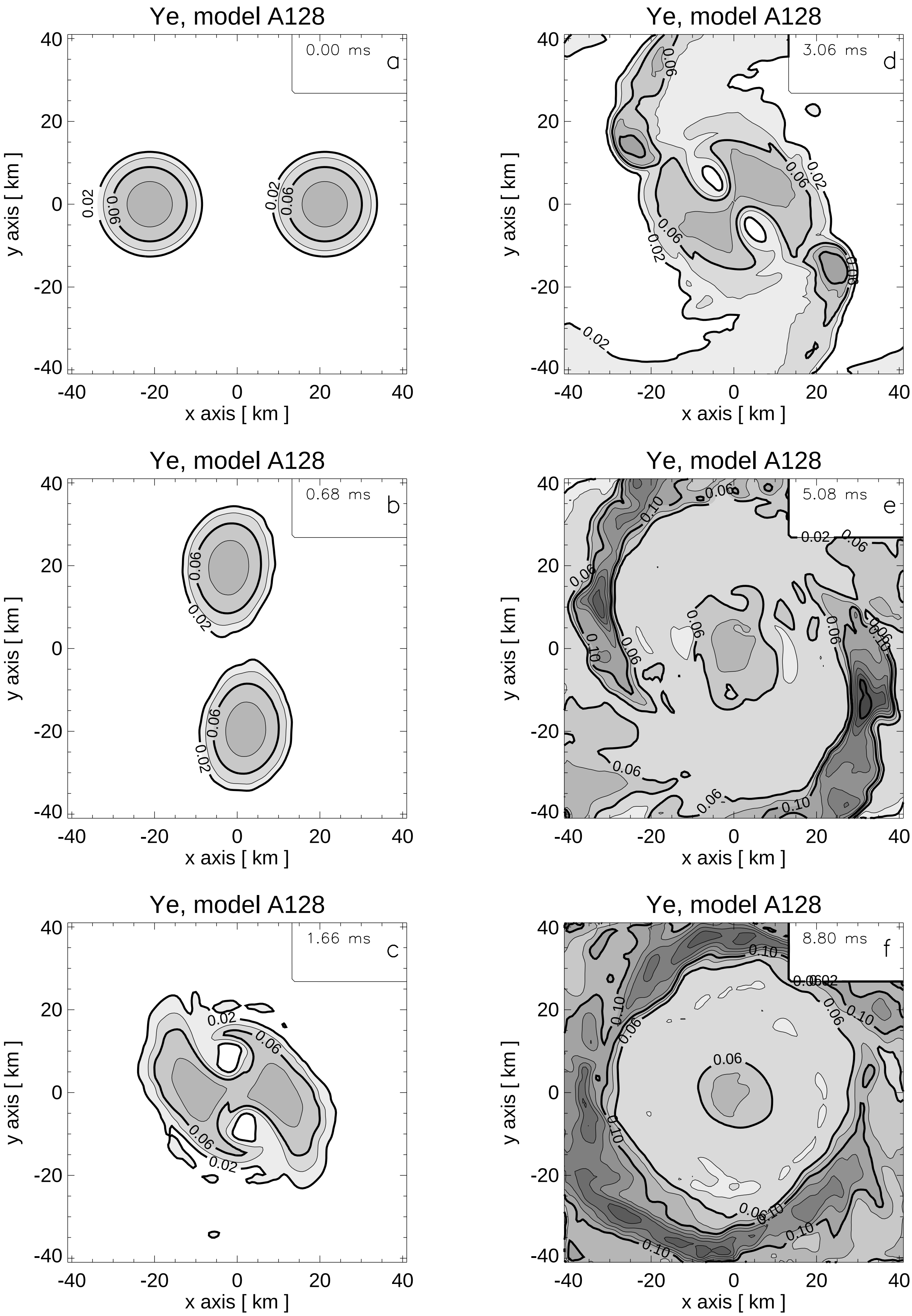

Fig. 13. Time evolution of the spatial distribution of the electron fraction Y_e in the orbital plane of model A128. The times of the snapshots are given in the upper right corners of the panels. The contours are linearly spaced with intervalls of 0.02, bold lines are labeled with their respective values, and the grey shading emphasizes the contrasts, higher values of Y_e being associated with darker grey

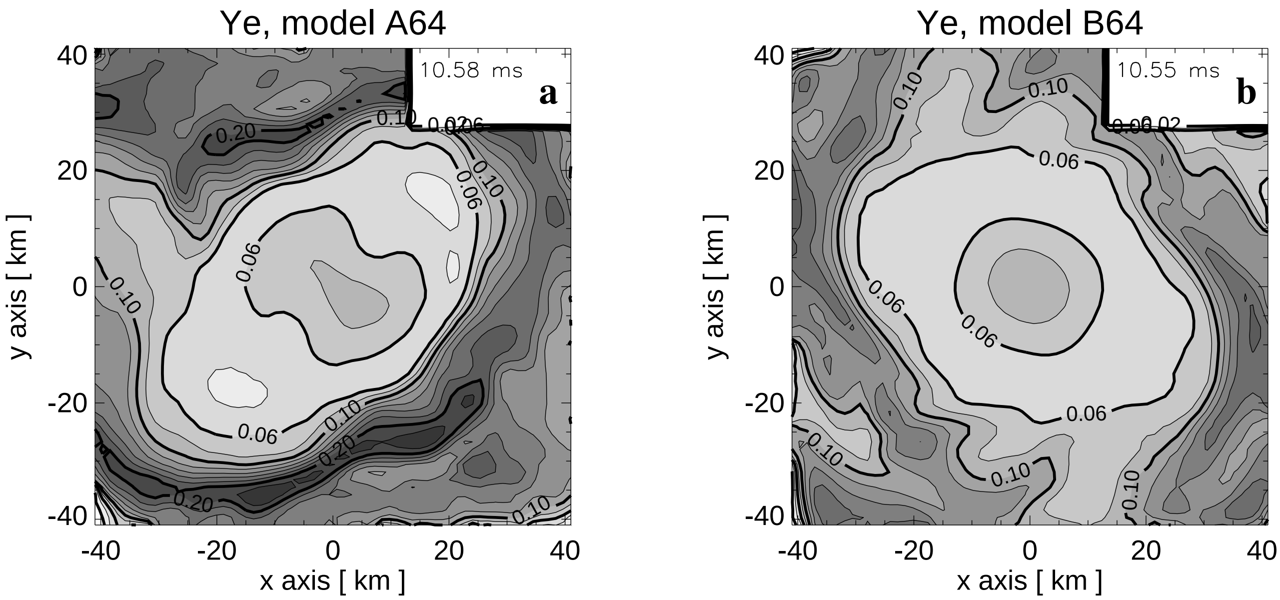

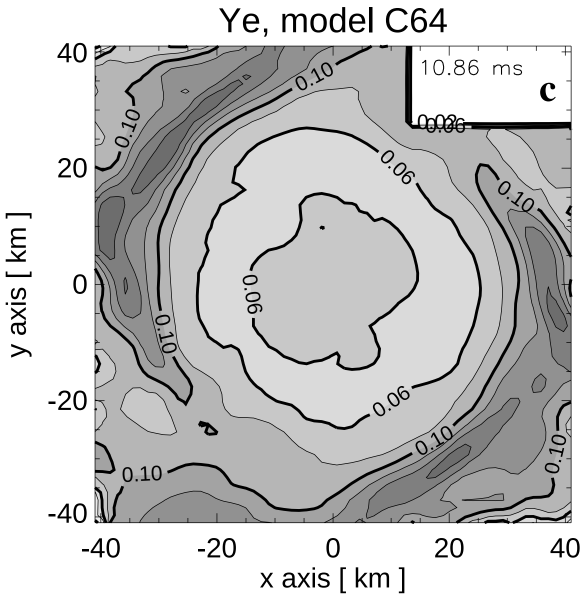

Fig. 14. The spatial distributions of the electron fraction Y_e in the orbital plane for models A64, B64, and C64 at the end of the calculations (times given in the top right corners). The contours are linearly spaced with intervalls of 0.02 and the bold contours are labeled with their respective values. The grey shading emphasizes the levels with darker shading indicating higher values of Y_e. The plots have to be compared with panel **f** of Fig. 13 which shows the same information for model A128 at time $t = 8.80$ ms

$k_{\rm B}T \gtrsim 6$ MeV where $\rho \gtrsim 10^{11}\,{\rm g/cm^3}$, and $k_{\rm B}T \gtrsim$ 1–2 MeV for $\rho \gtrsim 10^{10}\,{\rm g/cm^3}$. The corresponding entropies are less than 1 $k_{\rm B}$/nucleon in the core region and between 3 and slightly more than 7 $k_{\rm B}$/nucleon in the disk (panel **d**). In model C64 similar disk entropies are found while in model A64 specific entropies up to about 9 $k_{\rm B}$/nucleon and in model B64 up to even 10 $k_{\rm B}$/nucleon develop towards the end of the simulated evolution.

Such high entropies allow only minor contributions of nuclei to be present in the gas in nuclear statistical equilibrium at the densities found for the disk matter on our computational grid. Most of the nuclei are completely disintegrated into free nucleons (the mass fraction of heavy nuclei is below the lower limit of $\sim 10^{-8}$ returned from the equation of state of Lattimer & Swesty (1991)), and only small admixtures of α particles are possible. Panel **e** of Fig. 15 shows that the mass fraction X_α of α particles is typically less than about 10^{-3}. Only in the outermost parts of the disk $X_\alpha \sim 10^{-2}$ because there the temperatures are low enough, $k_{\rm B}T \sim$ 1–2 MeV, that some of the free nucleons can recombine.

4. Neutrino-antineutrino annihilation

Neutrino-antineutrino annihilation in the surroundings of the merger has been proposed to create a sufficiently energetic fireball of e^+e^--pairs and photons to explain gamma-ray bursts at cosmological distances. We attempt to put this idea to a quantitative test. With the given information about the fluxes and spectra of the neutrino emission of all grid cells (see Paper I for technical details), it is possible to evaluate our hydrodynamical

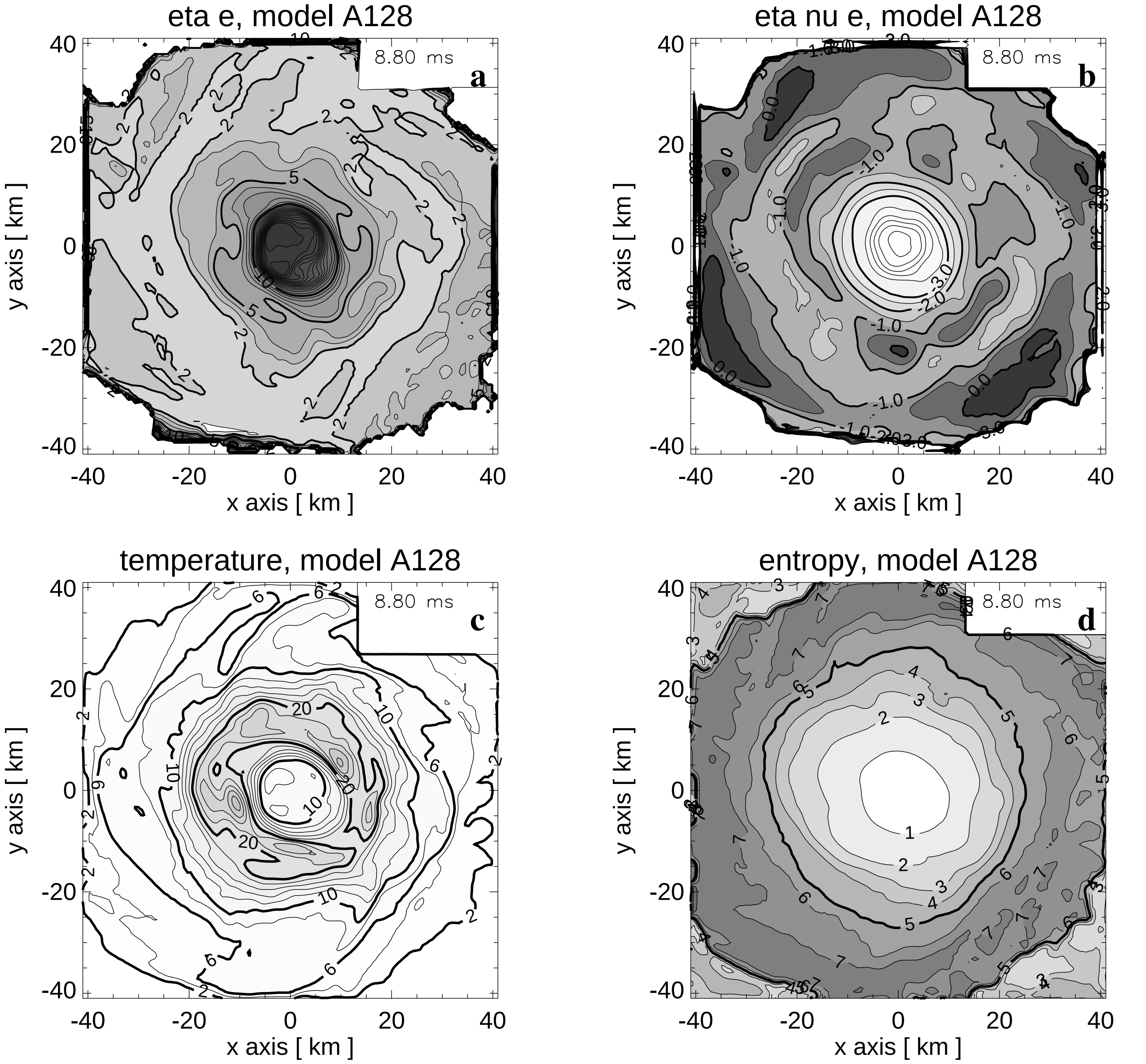

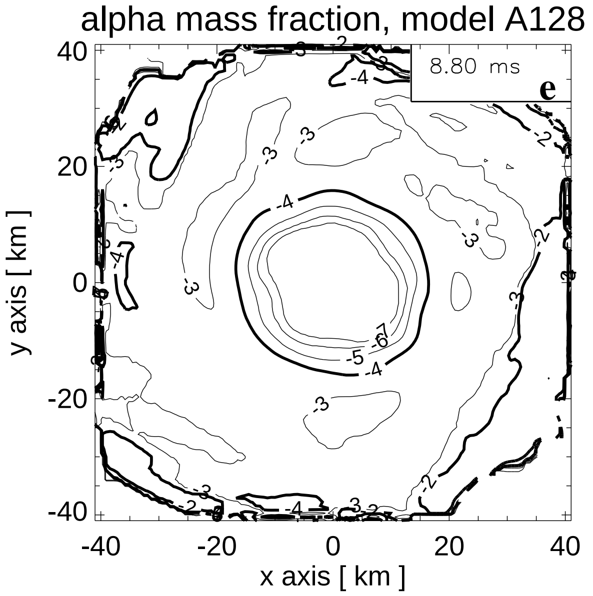

Fig. 15. Cuts in the orbital plane of model A128 showing different thermodynamical and composition parameters at the end of the simulated evolution (time $t = 8.80$ ms). Panel **a** gives the electron degeneracy parameter η_e (contours linearly spaced with steps of one unit), panel **b** shows the electron neutrino degeneracy parameter η_{ν_e} (contours linearly spaced with steps of 0.5 units), panel **c** displays the temperature distribution (contours linearly spaced with steps of 2 MeV), panel **d** is a plot of the entropy per nucleon (contours linearly spaced with steps of 1 $k_{\rm B}$/nucleon), and panel **e** informs about the mass fraction of α particles in the medium (contours logarithmically spaced in steps of one dex)

models for the energy deposition by $\nu\bar{\nu}$-annihilation in a post-processing step. Since the neutrino luminosities become large only after the merging of the two neutron stars and in particular after the gas torus around the compact central body has formed, we consider the late stages of our simulated merger evolutions as the most interesting ones to perform the analyses. In the phase when quasi-stationary conditions have been established, the neutrino luminosities have reached their saturation levels and the annihilation rates have become maximal.

4.1. Numerical evaluation

Neglecting phase space blocking effects in the phase spaces of e^- and e^+, the local energy deposition rate (energy $\mathrm{cm}^{-3}\mathrm{s}^{-1}$) at a position $\mathbf{r}$ by annihilation of ν_i and $\bar{\nu}_i$ into e^+e^--pairs (which is the dominant reaction between neutrinos and antineutrinos) can be written in terms of the neutrino and antineutrino phase space distribution functions $f_{\nu_i} = f_{\nu_i}(\epsilon, \mathbf{n}, \mathbf{r}, t)$ and $f_{\bar{\nu}_i} = f_{\bar{\nu}_i}(\epsilon', \mathbf{n}', \mathbf{r}, t)$ as (Goodman et al. 1987, Cooperstein et al. 1987, Janka 1991)

$$
\begin{aligned}
Q^+_{\nu\bar{\nu}}(\nu_i\bar{\nu}_i) = {} & \frac{1}{4}\,\frac{\sigma_0 c}{(m_e c^2)^2\,(hc)^6} \\
& \Bigg\{ \frac{(C_1+C_2)_{\nu_i\bar{\nu}_i}}{3} \cdot \int_0^\infty \mathrm{d}\epsilon \int_0^\infty \mathrm{d}\epsilon' \; (\epsilon+\epsilon')\; \epsilon^3 \epsilon'^3 \\
& \quad \oint_{4\pi} \mathrm{d}\Omega \oint_{4\pi} \mathrm{d}\Omega' \; f_{\nu_i} f_{\bar{\nu}_i} \; (1-\cos\theta)^2 \; + \\
& + \; C_{3,\nu_i\bar{\nu}_i}\,(m_e c^2)^2 \cdot \int_0^\infty \mathrm{d}\epsilon \int_0^\infty \mathrm{d}\epsilon' \; (\epsilon+\epsilon')\; \epsilon^2 \epsilon'^2 \\
& \quad \oint_{4\pi} \mathrm{d}\Omega \oint_{4\pi} \mathrm{d}\Omega' \; f_{\nu_i} f_{\bar{\nu}_i} \; (1-\cos\theta) \Bigg\} \, . \qquad (1)
\end{aligned}
$$

When the energy integrations are absorbed into (energy-integrated) neutrino intensities I_{ν_i} and $I_{\bar{\nu}_i}$,

$$
I_\nu \;=\; I_\nu(\mathbf{n},\mathbf{r},t) \;\equiv\; \frac{c}{(hc)^3} \int_0^\infty \mathrm{d}\epsilon \; \epsilon^3 \; f_\nu(\epsilon,\mathbf{n},\mathbf{r},t) \; , \qquad (2)
$$

Eq. (1) can be rewritten as

$$
\begin{aligned}
Q^+_{\nu\bar{\nu}}(\nu_i\bar{\nu}_i) = {} & \frac{1}{4}\,\frac{\sigma_0}{c\,(m_e c^2)^2} \Bigg\{ \frac{(C_1+C_2)_{\nu_i\bar{\nu}_i}}{3} \cdot \\
& \oint_{4\pi} \mathrm{d}\Omega\, I_{\nu_i} \oint_{4\pi} \mathrm{d}\Omega'\, I_{\bar{\nu}_i} \; [\langle\epsilon\rangle_{\nu_i} + \langle\epsilon\rangle_{\bar{\nu}_i}] \; (1-\cos\theta)^2 \; + \\
& + \; C_{3,\nu_i\bar{\nu}_i}\,(m_e c^2)^2 \cdot \\
& \oint_{4\pi} \mathrm{d}\Omega\, I_{\nu_i} \oint_{4\pi} \mathrm{d}\Omega'\, I_{\bar{\nu}_i} \; \frac{\langle\epsilon\rangle_{\nu_i} + \langle\epsilon\rangle_{\bar{\nu}_i}}{\langle\epsilon\rangle_{\nu_i}\,\langle\epsilon\rangle_{\bar{\nu}_i}} \; (1-\cos\theta) \Bigg\} \, . \qquad (3)
\end{aligned}
$$

The integrals over Ω and Ω' sum up neutrino and antineutrino radiation incident from all directions. θ is the angle between neutrino and antineutrino beams and $\langle\epsilon\rangle_{\nu_i}$ and $\langle\epsilon\rangle_{\bar{\nu}_i}$ are suitably defined average spectral energies of neutrinos and antineutrinos, respectively. The weak interaction cross section is $\sigma_0 = 1.76 \times 10^{-44}\,\mathrm{cm}^2$, $m_e c^2 = 0.511\,\mathrm{MeV}$ is the electron rest-mass energy, c the speed of light, and the weak coupling constants are $(C_1+C_2)_{\nu_e\bar{\nu}_e} = (C_V - C_A)^2 + (C_V + C_A)^2 \approx 2.34$, $C_{3,\nu_e\bar{\nu}_e} = \frac{2}{3}\left(2C_V^2 - C_A^2\right) \approx 1.06$ and $(C_1+C_2)_{\nu_x\bar{\nu}_x} = (C_V - C_A)^2 + (C_V + C_A - 2)^2 \approx 0.50$, $C_{3,\nu_x\bar{\nu}_x} = \frac{2}{3}\left[2(C_V-1)^2 - (C_A-1)^2\right] \approx -0.16$ for $\nu_x = \nu_\mu,\, \nu_\tau$ and $C_A = \frac{1}{2}$, $C_V = \frac{1}{2} + 2\sin^2\theta_\mathrm{W}$ with $\sin^2\theta_\mathrm{W} = 0.23$. The total energy deposition rate at the position $\mathbf{r}$ is given as the sum of the contributions from annihilation of ν_e and $\bar{\nu}_e$, ν_μ and $\bar{\nu}_\mu$, and ν_τ and $\bar{\nu}_\tau$:

$$
Q^+_{\nu\bar{\nu}}(\mathbf{r}) \;=\; Q^+_{\nu\bar{\nu}}(\nu_e\bar{\nu}_e) + Q^+_{\nu\bar{\nu}}(\nu_\mu\bar{\nu}_\mu) + Q^+_{\nu\bar{\nu}}(\nu_\tau\bar{\nu}_\tau) \, . \qquad (4)
$$

When working with a discrete grid the integrals in Eq. (3) are replaced by sums over all cells k,

$$
\oint_{4\pi} \mathrm{d}\Omega\, I_\nu \;\longrightarrow\; \sum_k \Delta\Omega_k \cdot I_{\nu,k} \, . \qquad (5)
$$

$\Delta\Omega_k$ is the solid angle with which cell k is seen from a position $\mathbf{r}$ at distance $d_k \equiv |\mathbf{r} - \mathbf{r}_k|$ when $\mathbf{r}_k$ is the location of the center of cell k. In order to avoid the need to take into account projection effects, we define an effective radius D associated with the cells of the cartesian grid used for the hydrodynamical modelling by setting the cell volume $V_k = \Delta x \Delta y \Delta z = (\Delta x)^3$ equal to the volume of a sphere $V = 4\pi D^3/3$:

$$
D \;=\; \left(\frac{3}{4\pi}\right)^{1/3} \Delta x \, . \qquad (6)
$$

With the projected area $A = \pi D^2$ we obtain

$$
\Delta\Omega_k \;=\; \pi \left(\frac{3}{4\pi}\right)^{2/3} \left(\frac{\Delta x}{d_k}\right)^2 \, . \qquad (7)
$$

Using the simplifying assumption that a grid cell radiates neutrinos with isotropic intensity into the half space around the outward direction defined by the local density gradient $\mathbf{n}_\rho = \nabla\rho/|\nabla\rho|$, the flux $j_{\nu_i,k}$ is related to the neutrino radiation intensity $I_{\nu_i,k}$ by $j_{\nu_i,k} = \pi I_{\nu_i,k}$. With an effective emissivity $Q_k^\mathrm{eff}(\nu_i)$ (see Paper I) which represents the energy emission of cell k per $\mathrm{cm}^{-3}\mathrm{s}^{-1}$ in a single neutrino species $\nu_i = \nu_e,\, \bar{\nu}_e,\, \nu_\mu,\, \bar{\nu}_\mu,\, \nu_\tau$ or $\bar{\nu}_\tau$, the intensity $I_{\nu_i,k}$ is therefore given by

$$
I_{\nu_i,k} = \frac{j_{\nu_i,k}}{\pi} = \frac{1}{\pi}\, Q_k^\mathrm{eff}(\nu_i)\, \frac{V}{A} = Q_k^\mathrm{eff}(\nu_i)\, \frac{4}{3\pi} \left(\frac{3}{4\pi}\right)^{1/3} \Delta x \, . \qquad (8)
$$

Eq. (7) and Eq. (8) allow us to evaluate the sum of Eq. (5) sufficiently accurately by

$$
\sum_k \Delta\Omega_k \cdot I_{\nu_i,k} \;\approx\; \frac{1}{\pi}\,(\Delta x)^3 \sum_k \frac{Q_k^\mathrm{eff}(\nu_i)}{d_k^2} \, . \qquad (9)
$$

With the average energy of neutrinos emitted from cell k, $\langle\epsilon\rangle_{\nu_i,k}$, (see Paper I) and the angle enclosed by the radiation from cells k and k' at the position $\mathbf{r}$, $\cos\theta_{kk'} =$

$(\mathbf{r}-\mathbf{r}_k)\,(\mathbf{r}-\mathbf{r}_{k'})\,/\,(d_k d_{k'})$, the integrals of Eq. (3) finally become sums over all combinations of grid cells k with all cells k'. This double sum has to be evaluated at all positions $\mathbf{r}$ where the energy deposition rate by $\nu\bar{\nu}$-annihilation is to be determined. The corresponding computational load is appreciable but can be significantly reduced by taking into account only those grid cells which emit towards $\mathbf{r}$, i.e. whose emission into the outward directed half space around $\mathbf{n}_\rho$ is also pointing to position $\mathbf{r}$. The criterion for this being fulfilled is $\mathbf{n}_\rho \cdot (\mathbf{r}-\mathbf{r}_k) > 0$.

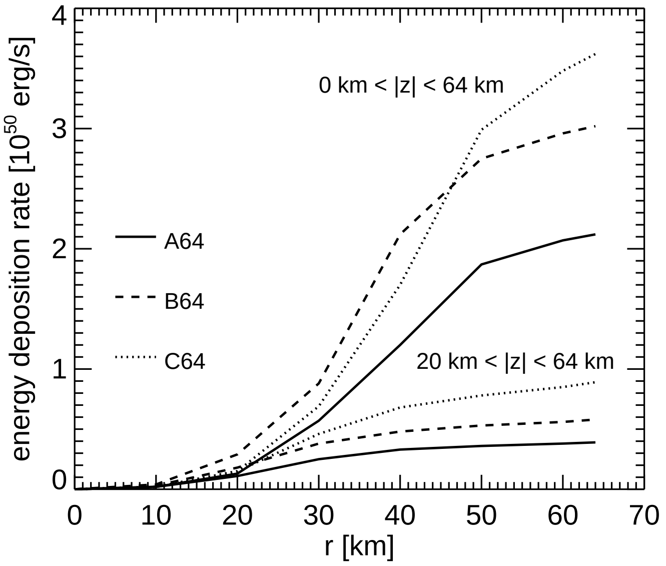

Fig. 17. Cumulative total energy deposition rates by neutrino-antineutrino annihilation into electron-positron pairs for the three models A64, B64, and C64 as functions of the equatorial distance r from the center of the merger once for the case that the integration is done for polar distances $20\,\mathrm{km} \le |z| \le 64\,\mathrm{km}$ and another time for $0\,\mathrm{km} \le |z| \le 64\,\mathrm{km}$. The integrals were performed over the values of the local energy deposition rates plotted in the three panels of Fig. 16

4.2. Numerical results

The numerical post-processing procedure described in the previous section yields the total energy deposition rate $Q^+_{\nu\bar{\nu}}$ by neutrino-antineutrino annihilation as a function of the position $\mathbf{r}$. Figure 16 shows the results, averaged over azimuthal angles, in a quadrant of the r-z-plane perpendicular to the orbital plane for the three models A64, B64, and C64. The evaluation was performed only in that region around the central part of the merger where the local energy loss rate by neutrino emission is less than $10^{30}\,\mathrm{erg/cm^3/s}$ and the density is below $10^{11}\,\mathrm{g/cm^3}$. Density levels are indicated by dashed contour lines in the plots.

One can see that in all three models the highest rate of energy deposition ($> 10^{30}\,\mathrm{erg/cm^3/s}$) occurs in the outer regions of the disk ($35\,\mathrm{km} \le r \le 45\,\mathrm{km}$ in the orbital plane) within about 25 km above and below the orbital plane. Here the energy deposition rate is much larger than the energy loss rate. Because this deposition transfers energy into gas layers with densities of still more than $10^{10}\,\mathrm{g/cm^3}$, one must suspect that a baryonic wind will be created very similar to the neutrino-driven wind caused by neutrino energy deposition in the surface layers of the nascent neutron star in a type-II supernova (for information about the neutrino-driven wind from forming neutron stars, see Duncan et al. 1986, Woosley & Baron 1992, Witti et al. 1994, Woosley et al. 1994; see also Hernanz et al. 1994). Instead of creating a fireball of a nearly pure relativistic electron-positron-photon plasma which might lead to an energetic gamma-ray burst, this energy is used up to lift baryons in the strong gravitational field of the massive central body. Consequently, the expansion velocities of this matter are nonrelativistic. If too much of this wind material gets mixed into the pair-photon plasma, the baryonic load M_w can become too high to allow for Lorentz factors Γ in the required range of $\Gamma = 1/\sqrt{1-(v/c)^2} \sim E_{\nu\bar{\nu}}/(M_\mathrm{w}c^2) \gtrsim 100$.

The large energy deposition rates at radii between 30 km and 50 km in the equatorial plane and at moderate heights above and below the orbital plane can be explained by the closeness to the main neutrino emitting ring in the disk between 20 km and 30 km (see Figs. 5–10). According to Eqs. (3), (5), and (9) the annihilation rate decreases at least with the fourth power of the distance to the neutrino radiating grid cells k and k': $Q^+_{\nu\bar{\nu}} \propto 1/(d_k^2 d_{k'}^2)$. Because of the influence of the geometrical factor $(1-\cos\theta)^2$ in Eq. (3) (this factor accounts for the dependence of the annihilation probability on the relative velocity of the interacting neutrinos and the kinematically allowed phase space for the reaction), $Q^+_{\nu\bar{\nu}}$ decreases even more steeply when one moves away from the source and large-θ collisions between neutrinos become less and less frequent. At distances from the merged object $d \equiv \sqrt{r^2+z^2} \gtrsim 50$–$60$ km we find that along each radial beam the local energy deposition rate as a function of d becomes a power law with power law index between -6 and -8. Towards the rotation (z-) axis, the growing distance to the neutrino producing disk region cannot be compensated by the higher chance of head-on collisions between neutrinos. This is the reason why the contour levels in the plots of Fig. 16 bend towards the polar region of the merger near the z-axis.

The integral values of the energy deposition rate by $\nu\bar{\nu}$-annihilation in the surroundings of the merger out to equatorial distances r are shown in Fig. 17. For each of the models A64, B64, and C64 we have evaluated the spatial integral once for vertical heights 20 km $\le |z| \le$ 64 km and another time for 0 km $\le |z| \le$ 64 km. The maximum upper integration limit is determined by the largest distances where the local rates $Q^+_{\nu\bar{\nu}}$ were calculated. However, one can see from Fig. 17 that the curves tend to approach a saturation level for $r \to 64$ km from which we conclude that extending the integrations into the region $d > 64$ km would not change the results significantly. From a comparison of both cases one can recognize that only a minor fraction of about $1/5$–$1/4$ of the annihilation energy is converted into e^+e^--pairs in the region above and below the disk. Only at heights $|z| \gtrsim 20$ km is the baryon density low enough that most of the converted energy might end up in a rel-

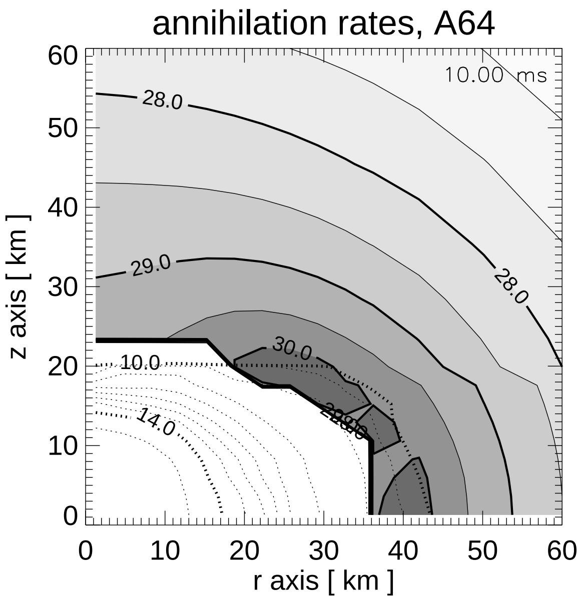

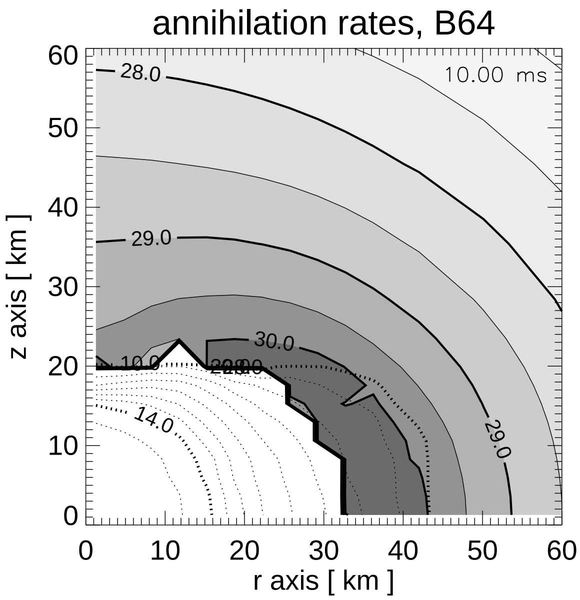

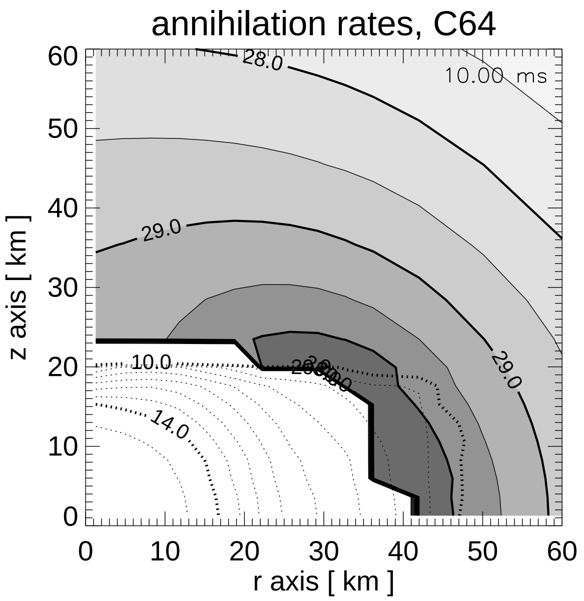

Fig. 16. Maps of the total local energy deposition rates (in erg/cm^3/s) by neutrino-antineutrino annihilation into electron-positron pairs in the vicinity of the merger for the three models A64, B64, and C64 at time $t = 10$ ms after the start of the simulations. In one quadrant of the r-z plane orthogonal to the orbital plane (at $z = 0$), the plots show values obtained as averages of the energy deposition rate over azimuthal angles. The corresponding solid contour lines are logarithmically spaced in steps of 0.5 dex, the grey shading emphasizes the levels with dark grey meaning high energy deposition rate. The dashed contours indicate levels of the azimuthally averaged density, also logarithmically spaced with intervals of 0.5 dex. The energy deposition rate was evaluated only in that region around the merged object, where the mass density is below 10^{11} g/cm^3 *and* the energy loss rate by neutrino emission is smaller than 10^{30} erg/cm^3/s. One can see that due to the closeness to the main neutrino radiating disk region, most annihilation energy is deposited in the "outer" (in r-direction) and "upper" (in z-direction) regions of the disk (dark grey areas)

ativistic fireball. However, in the whole region $0\ \mathrm{km} \leq |z| \leq 64\ \mathrm{km}$ the energy deposition rate is rather small, only about 2–$4 \cdot 10^{50}\,\mathrm{erg/s}$; the "useful" fraction is probably less than $1/4$ of that. The models were evaluated at times when the neutrino emission of the models had already achieved a maximum value and a quasi-stationary state. At earlier times the neutrino luminosities are much lower and therefore the integral values of the energy deposition rate are even smaller than those displayed in Fig. 17.

For the disk or torus geometry of our models the annihilation efficiency, defined as $e_{\nu\bar{\nu}} \equiv (\mathrm{d}E_{\nu\bar{\nu}}/\mathrm{d}t)/(L_{\nu_e} + L_{\bar{\nu}_e} + 4L_{\nu_\mu})$ where $\mathrm{d}E_{\nu\bar{\nu}}/\mathrm{d}t$ is the total energy deposition rate by $\nu\bar{\nu}$-annihilation, can be found to be of the order of a few tenths of a per cent:

$$e_{\nu\bar{\nu}} = (2 \ldots 3) \cdot 10^{-3}\, \frac{L_{\nu_e}}{1.5 \cdot 10^{52}\mathrm{erg/s}}\, \frac{\langle\epsilon_{\nu_e}\rangle}{13\,\mathrm{MeV}}\, \frac{20\,\mathrm{km}}{R_\mathrm{d}}\ . \quad (10)$$

The factors in this equation can be deduced by simple analytical transformations and dimensional considerations of the volume integral of the annihilation rate (Eq. (10)). R_d is the inner radius of the disk, the radius which roughly separates the compact inner core from the more dilute gaseous cloud of matter around. The inserted numbers are representative values taken from Figs. 1, 3, and 4. The efficiency of Eq. (10) for converting emitted neutrino energy into electron-positron pairs by $\nu\bar{\nu}$-annihilation is in good agreement with what is obtained in supernova simulations or analytical estimates assuming emission in a spherical geometry instead of the disk-dominated emission of our numerical models.

From the results discussed here we conclude that there is no chance to obtain the energies needed for a cosmological gamma-ray burst by $\nu\bar{\nu}$-annihilation during the instant of the merging of binary neutron stars. Before the hot cloud of gas around the central, dense body has formed, the neutrino luminosities stay rather low and only very little energy is deposited by $\nu\bar{\nu}$-annihilation. Even later when a disk around the compact, merged body has formed and the neutrino emission has reached a high level, the energy deposition rates of 2–$4 \cdot 10^{50}\,\mathrm{erg/s}$ lead to a total deposited energy of only a few $10^{48}\,\mathrm{erg}$ within the computed time of 10 ms. One would need the strong neutrino emission to be maintained for periods of about 10 s to pump an energy of more than $10^{51}\,\mathrm{erg}$ into a fireball of e^+e^--pairs and photons. Note that these statements are *not* changed if the observed gamma-ray bursts are beamed events. If one relies on the emission geometry of our models, a constrained solid angle $\Delta\Omega$ into which the fireball expands and becomes visible in a jet-like outburst would also (and by the same factor) reduce the spatial volume where $\nu\bar{\nu}$-annihilation in the surroundings of the merger could deposit the useful energy. Correspondingly, the numbers given in Fig. 17 would have to be scaled down by a factor $\Delta\Omega/(4\pi)$. In view of the fact discussed in Sect. 2.3 that the central, compact core of the merger has a mass that can neither be stabilized by internal pressure nor by rotation and should therefore collapse into a black hole on a time scale of milliseconds, we conclude that the energy available by pair annihilation of neutrinos is lower than the desired and required "canonical" value of $10^{51}/(4\pi)\,\mathrm{erg/steradian}$ by more than a factor of 1000.

So far we have considered the phase of the merging of binary neutron stars and the evolution that follows immediately afterwards. This, however, leaves the question unanswered whether a disk around the most likely forming black hole could produce and emit neutrinos on a much longer time scale and could thus power a gamma-ray burst by the discussed mechanism of neutrino-pair annihilation? Since simulations of this scenario are beyond the present capabilities of the employed numerical code and, in addition, the results depend on the unknown viscosity in the disk, we attempt to develop a simple model of the behavior and properties of such a disk with respect to its neutrino emission and the strength of $\nu\bar{\nu}$-annihilation.

4.3. Simple model for the post-merging emission from the disk

Our simulations suggest that some material, possibly about $0.1\,M_\odot$, could remain in a disk around the central black hole. This disk will be heated by viscous dissipation and will emit neutrinos and antineutrinos until its matter is accreted into the central black hole. The efficiency of $\nu\bar{\nu}$-annihilation increases linearily with the ν luminosity (Eq. (10)) and thus a short, very luminous neutrino burst is more efficient to create an e^+e^--pair fireball than the same energy emitted on a longer time scale with smaller neutrino fluxes. It has to be investigated whether enough energy can be provided in the pair-photon fireball by the neutrino emission from the disk to explain a γ-ray burst at cosmological distances. Viscosity effects have a crucial influence on the disk evolution and on the neutrino emission. Viscous forces, on the one hand, transfer angular momentum between adjacent fluid elements and determine the accretion time scale and accretion rate. Viscous dissipation of rotational energy, on the other hand, heats the disk and is thus essential for the neutrino emission. Disk size, disk temperature, disk viscosity, and neutrino emission properties can therefore not be chosen independent of the accretor mass and disk mass. In the following we shall attempt to relate these quantities by simple considerations and conservation arguments.

The lifetime of the disk will decrease with larger dynamic viscosity η because the viscous force that generates a torque carrying angular momentum outward is increased. For a (Newtonian) Keplerian disk the viscous force (per unit area) in the angular (ϕ) direction, f_ϕ, is simply expressed by the component $t_{r\phi}$ of the viscous stress tensor (see, e.g., Shapiro & Teukolsky 1983):

$$f_\phi = -t_{r\phi} = \frac{3}{2}\,\eta\,\Omega_\mathrm{k}\,, \tag{11}$$

where $\Omega_\mathrm{k} = \sqrt{GM/r^3}$ is the Keplerian angular velocity. The torque T exerted by the viscous stress is given by $T = f_\phi\, r\,(2\pi r\, 2h)$ when $2h \sim 2R_\mathrm{s}$ is taken as the vertical diameter of the thick disk around the black hole with mass M and Schwarzschild radius $R_\mathrm{s} = 2GM/c^2 \approx 9(M/3\,M_\odot)\,\mathrm{km}$. The accretion rate $\mathrm{d}M/\mathrm{d}t$ can be estimated (roughly) by setting the viscous torque equal to the rate $\mathrm{d}J/\mathrm{d}t \sim (\mathrm{d}M/\mathrm{d}t)\Omega_\mathrm{k}r^2$ at which angular momentum is consumed by the black hole due to the accretion of matter from the disk:

$$\frac{\mathrm{d}M}{\mathrm{d}t} \approx 6\pi\eta R_\mathrm{s}\,. \tag{12}$$

From that, the accretion time scale of a disk of mass ΔM_d is estimated to be

$$t_\mathrm{acc} \approx \frac{\Delta M_\mathrm{d}}{6\pi\eta R_\mathrm{s}}\,. \tag{13}$$

Thus, the lifetime of the disk is determined by the outward transport of angular momentum through the viscous torque. Equation (13) shows that it decreases with the value of the dynamic viscosity as $1/\eta$.

Viscous dissipation generates heat in the disk at a rate per unit volume of (see Shapiro & Teukolsky 1983)

$$\frac{\mathrm{d}Q}{\mathrm{d}t} = \frac{-f_\phi t_{r\phi}}{\eta} = \frac{9}{4}\,\eta\,\Omega_\mathrm{k}^2\,. \tag{14}$$

At steady-state conditions the maximum dissipation rate occurs at a radius $r \approx 1.36\,R_\mathrm{d} \approx \frac{4}{3}\,R_\mathrm{d}$ when R_d is the inner radius of the disk which is taken to be the innermost stable circular orbit around the central accreting black hole, $R_\mathrm{d} \approx 3R_\mathrm{s} \approx 6GM/c^2$. Using this in Eq. (14) one obtains for the maximum rate at which frictional heat is liberated,

$$\frac{\mathrm{d}Q}{\mathrm{d}t} \approx \frac{1}{28}\,\eta\,\frac{GM}{R_\mathrm{s}^3}\,. \tag{15}$$

Thus, the viscous heating rate increases linearly with η.

For small viscosity η the viscous heating time scale is long and the disk remains rather cool, also because cool matter is comparatively transparent for neutrinos and therefore the neutrino cooling time scale is short. In that case the neutrino luminosity for a disk with volume V_d is $L_\nu \sim V_\mathrm{d}\, \mathrm{d}Q/\mathrm{d}t \propto \eta$ and the total energy radiated in neutrinos, $E_\nu \sim L_\nu t_\mathrm{acc}$, becomes independent of η because of $t_\mathrm{acc} \propto 1/\eta$. With Eq. (10) one finds that the energy converted into e^+e^- by $\nu\bar\nu$-annihilation increases proportional to η: $E_{\nu\bar\nu} = e_{\nu\bar\nu} E_\nu \propto L_\nu^2 t_\mathrm{acc} \propto \eta$. In the optically thin case the mean energy of emitted neutrinos, $\langle\epsilon_\nu\rangle$, which enters the calculation of $e_{\nu\bar\nu}$ will also increase with η and cause a slightly steeper than linear dependence of $E_{\nu\bar\nu}$ on η.

If η is large, the disk is heated rapidly and strongly and thus becomes opaque for neutrinos. With a neutrino diffusion time scale t_diff that is much longer than the heating time scale the neutrino luminosity is $L_\nu \sim V_\mathrm{d}\, (\mathrm{d}Q/\mathrm{d}t) t_\mathrm{acc}/t_\mathrm{diff}$ which is only indirectly dependent on η through t_diff and thus the (viscosity dependent) gas temperature T. In that case $E_\nu \propto 1/(\eta t_\mathrm{diff})$ and $E_{\nu\bar\nu} \propto 1/(\eta t_\mathrm{diff}^2)$. Note that the average energy of emitted neutrinos, $\langle\epsilon_\nu\rangle$, which also determines $e_{\nu\bar\nu}$, is only very weakly dependent on the viscosity of the disk in the optically thick case because it reflects the conditions at the neutrino decoupling sphere (see Eq. (21) below). The diffusion time scale increases with the disk temperature and thus with the disk viscosity due to the energy dependence of the weak interaction cross sections. This leads to a decrease of $E_{\nu\bar\nu}$ with η that is steeper than $1/\eta$.

The considerations above suggest that the annihilation energy $E_{\nu\bar\nu}$ has a pronounced maximum at a particular value η^* of the dynamic viscosity. Because of $E_{\nu\bar\nu} \propto L_\nu^2$ the annihilation of neutrinos and antineutrinos is more efficient when a certain energy is emitted in a short time with a high luminosity rather than over a long period with a moderate flux. If η is small, L_ν stays low. If η is very large and the interior of the disk very hot and thus neutrino-opaque, the neutrino luminosity L_ν scales with the inverse of the neutrino diffusion time scale and with the total energy E_ν that can be emitted in neutrinos during the lifetime t_acc of the disk. This energy E_ν decreases in case of very large η because t_acc becomes shorter and the internal energy cannot be completely radiated away in neutrinos before the neutrino-opaque matter is accreted into the black hole. The kinetic energy that is converted into internal energy by viscous friction is entirely transported away by neutrinos and the fluxes are largest, if the diffusion time scale is similar to the accretion time scale but not much longer. The optimum value η^* is therefore determined by the condition $t_\mathrm{acc} \approx t_\mathrm{diff}$.

Let us assume that the part of the disk where most of the neutrinos are emitted has a mass ΔM_d and is a homogeneous torus with center at $4R_\mathrm{s}$ and radius R_s (inner radius $3R_\mathrm{s}$, outer radius $5R_\mathrm{s}$) (Mochkovitch et al. 1993; Jaroszyński 1993). This is a fairly good picture in view of the shape and structure of the disk that we obtained in our numerical simulations[1]. In terms of R_s the volume of the disk torus is $V_\mathrm{d} = 8\pi^2 R_\mathrm{s}^3$ and its surface $S_\mathrm{d} = 16\pi^2 R_\mathrm{s}^2$. With the neutrino mean free path $\lambda = \rho\sigma_\mathrm{eff}/m_u$ and $\Delta M_\mathrm{d} = \rho V_\mathrm{d}$ the diffusion time scale is approximately given by

$$t_\mathrm{diff} \sim \frac{3R_\mathrm{s}^2}{c\lambda} \sim \frac{3(\Delta M_\mathrm{d})\sigma_\mathrm{eff}}{8\pi^2 R_\mathrm{s} m_\mathrm{u} c}\,. \tag{16}$$

Here m_u is the atomic mass unit and the thermally averaged effective neutrino interaction cross section $\sigma_\mathrm{eff} \equiv \sum_i Y_i\sigma_i$ is defined as the sum of the cross sections σ_i times the number fractions $Y_i = n_i/n_B$ of the corresponding reaction targets for all neutrino processes in the medium, i.e., neutrino scattering off n, p, e^-, e^+, charged-current absorptions of ν_e and $\bar\nu_e$ by n and p, respectively, and ν-pair interactions. We find

$$\sigma_\mathrm{eff} \sim (1 \ldots 4)\cdot 10^{-41} \left(\frac{k_\mathrm{B}T}{5\,\mathrm{MeV}}\right)^2 \mathrm{cm}^2\,, \tag{17}$$

the exact value depending on the neutrino type, the neutrino degeneracy and neutrino spectra, and the detailed composition of the medium. For the entropies, densities, and temperatures obtained in our simulations the gas in the disk is completely disintegrated into free nucleons; nucleon as well as lepton degeneracy plays a negligible role (see Sect. 3.2). Therefore fermion phase space blocking effects are unimportant. The thermal average of the neutrino cross section was evaluated by using a Fermi-Dirac distribution function with a vanishing neutrino chemical potential, $\mu_\nu = 0$. In case of incomplete dissociation of the nuclei the neutrino opacity should still be within the uncertainty range associated with the cross section variation of Eq. (17). Setting t_acc (Eq. (13)) with $\Delta M_\mathrm{d} = \rho V_\mathrm{d}$ equal to t_diff (Eq. (16)), one determines the value of the shear viscosity in the disk, where $\nu\bar\nu$-annihilation yields the largest energy, as

$$\eta^* \approx \frac{4\pi}{9}\,\frac{m_\mathrm{u}c}{\sigma_\mathrm{eff}} \sim (1.7 \ldots 6.9)\cdot 10^{27} \left(\frac{k_\mathrm{B}T}{5\,\mathrm{MeV}}\right)^{-2} \frac{\mathrm{g}}{\mathrm{cm\,s}}\,. \tag{18}$$

The range of values accounts for the uncertainty in the effective neutrino interaction cross section. For the typical composition of the disk material the cross section is more likely near the upper limit of the given interval, in which case the lower value of η^* is favored.

Let us now consider a disk with this optimum value η^*. Making use of η^*, the interior temperature of the disk can be estimated by setting the integral rate of viscous energy generation in the disk, $L_\mathrm{visc} \sim V_\mathrm{d}(\mathrm{d}Q/\mathrm{d}t)$, equal to the luminosity due to neutrino diffusion, $L_\nu \sim V_\mathrm{d}\varepsilon_\nu/t_\mathrm{diff} \sim (\frac{1}{3}c\lambda)S_\mathrm{d}(\varepsilon_\nu/R_\mathrm{s})$. Here $\varepsilon_\nu/R_\mathrm{s}$ is an approximation to the gradient of the neutrino energy density in the disk and $\varepsilon_\nu \sim 3\cdot\frac{7}{8}a_\mathrm{rad}T_\mathrm{int}^4$ is the sum of the energy densities of all three kinds of non-degenerate $\nu\bar\nu$-pairs with a_rad being the radiation constant. One finds

$$\frac{k_\mathrm{B}T_\mathrm{int}}{5\,\mathrm{MeV}} \approx 5.6\,(\Delta M_\mathrm{d,01})^{1/4} R_\mathrm{s,9}^{-3/4} \tag{19}$$

[1] In the simple model considered here, the structure and geometry of the disk is assumed to be given. It is not self-consistently determined in dependence of the gas temperature and thus in dependence of the competing effects of viscous heating and neutrino cooling.

where $\Delta M_{\rm d,01} \equiv \Delta M_{\rm d}/(0.1\,M_\odot)$ and $R_{\rm s,9} \equiv R_{\rm s}/(9\,{\rm km})$ is normalized to the Schwarzschild radius of a $3\,M_\odot$ black hole. Note that due to the dependence of $t_{\rm diff}$ and of η^* on $\sigma_{\rm eff}$ (according to Eqs. (16) and (18), respectively) $k_{\rm B}T_{\rm int}$ does not depend on the neutrino interaction cross section and is therefore insensitive to its uncertainty.

Plugging the result of Eq. (19) for the interior disk temperature into Eq. (18) yields for the optimum disk viscosity

$$\eta^* \sim (5.5\,...\,22)\cdot 10^{25}\,(\Delta M_{\rm d,01})^{-1/2}\,R_{\rm s,9}^{3/2}\;\frac{\rm g}{\rm cm\,s}\,, \qquad (20)$$

the interval of values again corresponding to the range of possible values of the effective neutrino interaction cross section. η^* from Eq. (20) can now be used in Eq. (15) to calculate $L_{\rm visc} \sim V_{\rm d}({\rm d}Q/{\rm d}t)$, which, when set equal to the neutrino luminosity expressed in terms of temperature and surface area $S_{\rm d}$ of the neutrinosphere, $L_\nu \sim S_{\rm d}(3\frac{7}{8}a_{\rm rad}T_{\rm surf}^4)c/4$, leads to an estimate of the neutrinospheric temperature

$$\frac{k_{\rm B}T_{\rm surf}}{5\,{\rm MeV}} \approx (0.7\,...\,1.0)\cdot(\Delta M_{\rm d,01})^{-1/8}\,R_{\rm s,9}^{1/8}\,. \qquad (21)$$

The temperature of the neutrino emitting disk surface is around 5 MeV and rather insensitive to the exact value of the effective neutrino interaction cross section (slightly larger result for smaller cross section), to the disk mass $M_{\rm d}$, and to the inner disk radius $R_{\rm d} \sim 3R_{\rm s}$.

The optimum value η^* for the dynamic viscosity as given in Eq. (20) corresponds to an effective α-parameter of $\alpha \approx \eta^*/(\rho c_{\rm s}R_{\rm s}) \sim (1.7\,...\,7.0)\cdot 10^{-3}$ when $R_{\rm s} = 9\,{\rm km}$, $\Delta M_{\rm d} = 0.1\,M_\odot$, and $\rho = \Delta M_{\rm d}/(8\pi^2 R_{\rm s}^3) = 3.44\cdot 10^{12}\,{\rm g/cm^3}$ are used, and the sound speed $c_{\rm s}$ is evaluated with $k_{\rm B}T = 28\,{\rm MeV}$. For these values of density and temperature the gas pressure is dominated by relativistic particles, i.e., photons, electrons, positrons, and neutrinos. Neutrino shear viscosity does not contribute significantly to η^*. In the neutrino-opaque case it is estimated to be

$$\eta_\nu = \frac{1}{3}\frac{\varepsilon_\nu\lambda}{c} = \frac{\varepsilon_\nu m_{\rm u}}{3\rho\sigma_{\rm eff}c}$$
$$\sim (1\,...\,4)\cdot 10^{23}\left(\frac{k_{\rm B}T}{5\,{\rm MeV}}\right)^2\left(\frac{10^{12}\,{\rm g/cm^3}}{\rho}\right)\;\frac{\rm g}{\rm cm\,s}\,, \qquad (22)$$

where the interval of the numerical value is again associated with the uncertainty of the effective cross section $\sigma_{\rm eff}$. For $\rho = 3.44\cdot 10^{12}\,{\rm g/cm^3}$ and $k_{\rm B}T = 28\,{\rm MeV}$ one finds $\eta_\nu \sim (0.9\,...\,3.6)\cdot 10^{24}\,{\rm g\,cm^{-1}s^{-1}}$. A temperature as high as $k_{\rm B}T \sim$ 70–80 MeV is required for the neutrino viscosity to become large enough to account for η^*.

For the diffusion and accretion time scales one obtains by inserting Eq. (20) into Eq. (13)

$$t_{\rm acc} \approx t_{\rm diff} \sim (53\,...\,212)\,(\Delta M_{\rm d,01})^{3/2}\,R_{\rm s,9}^{-5/2}\;{\rm ms}\,. \qquad (23)$$

This time is much longer than the dynamical time scale ($\mathcal{O}(1\,{\rm ms})$) and the neutrino equilibration time scale ($\lesssim 1\,{\rm ms}$). Therefore our assumptions that neutrinos diffuse in the disk and are in equilibrium with the matter are confirmed a posteriori. The total neutrino luminosity is

$$L_\nu \sim (0.62\,...\,2.48)\cdot 10^{53}(\Delta M_{\rm d,01})^{-1/2}R_{\rm s,9}^{5/2}\;{\rm erg/s}\,. \qquad (24)$$

In Eq. (23) the smaller values and in Eq. (24) the larger ones correspond to the case of larger viscosity η^* and thus smaller neutrino cross section $\sigma_{\rm eff}$ according to the postulated equality of Eqs. (13) and (16). The total energy $E_\nu = L_\nu t_{\rm acc}$ radiated away over the time $t_{\rm acc}$ is independent of both and becomes

$$E_\nu \approx \frac{\pi}{7}\frac{GM(\Delta M_{\rm d})}{3R_{\rm s}} = \frac{\pi}{42}(\Delta M_{\rm d})c^2$$
$$\approx 1.3\cdot 10^{52}\Delta M_{\rm d,01}\;\;{\rm erg} \qquad (25)$$

which is (approximately) equal to the Newtonian gravitational binding energy $E_{\rm bind} = \frac{1}{2}GM(\Delta M_{\rm d})/R_{\rm d} = |E_{\rm grav}+E_{\rm rot}|$ of mass $\Delta M_{\rm d}$ at the inner disk radius $R_{\rm d} = 3R_{\rm s}$ where the matter is swallowed by the black hole ($E_{\rm grav}$ is the gravitational potential energy, $E_{\rm rot}$ the rotational energy). Here it is assumed that no rotational kinetic energy is extracted from the black hole which is equivalent to a zero stress boundary condition at $R_{\rm d}$. This requires that within $R_{\rm d}$ the gas spirals into the black hole rapidly without radiating, an idealization which is probably justified (see, e.g., Shapiro & Teukolsky 1983). The small discrepancy between the factors $\frac{1}{2}$ and $\frac{\pi}{7}$ of our calculation results from the fact that we consider a simple one-zone model of a homogeneous disk. We find that the radiation efficiency of the disk in our simplified treatment is $E_\nu/(\Delta M_{\rm d}c^2) = \frac{\pi}{42} \approx 7.5\%$ (exact value for a thin, Newtonian accretion disk: $\frac{1}{12} \approx 8.3\%$). This result has to be compared with the radiation efficiency of about 5.7% for relativistic disk accretion onto a nonrotating black hole and with the radiation efficiency of 42.3% for a maximally rotating black hole with a prograde accretion disk (see Shapiro & Teukolsky 1983). Since our numerical simulations suggest the formation of a central black hole with a relativistic rotation parameter $a = Jc/(GM)$ that is clearly less than 1 (Ruffert et al. 1996), the reference value for the radiation efficiency for disk accretion onto a nonrotating black hole is relevant and our Newtonian disk evolution model most likely overestimates the amount of energy that can be carried away by neutrinos before the accreted mass finally plunges rapidly from $R_{\rm d}$ to the event horizon.

Using the results of Eqs. (21) and (24) to compute the $\nu\bar\nu$-annihilation efficiency $e_{\nu\bar\nu}$ according to Eq. (10) and employing the integral energy E_ν emitted in neutrinos as given from Eq. (25), one can obtain a result for the energy $E_{\nu\bar\nu} = e_{\nu\bar\nu}E_\nu$ deposited in an e^+e^--pair-photon fireball by the annihilation of ν and $\bar\nu$ radiated from the disk. With $R_{\rm d} = 3R_{\rm s} = 27\,{\rm km}$, $\langle\epsilon_{\nu_e}\rangle \approx 3k_{\rm B}T_{\rm surf} \sim (10.5\,...\,15.0)\,{\rm MeV}$, and $L_{\nu_e} \sim \left(\frac{1}{8}\,...\,\frac{1}{6}\right)L_\nu$ (see Sect. 3.1), i.e, $L_{\nu_e} \lesssim (1\,...\,4)\cdot 10^{52}\,{\rm erg/s}$, we get

$$E_{\nu\bar\nu} \sim (1.1\,...\,9.4)\cdot 10^{49}\,(\Delta M_{\rm d,01})^{3/8}\,R_{\rm s,9}^{13/8}\;{\rm erg}\,. \qquad (26)$$

The upper and lower bounds of the interval for $E_{\nu\bar\nu}$ correspond to the most extreme (maximum and minimum, respectively) choices for $e_{\nu\bar{\nu}}$, L_{ν_e}, and $\langle\epsilon_{\nu_e}\rangle$. Notice that the analytical estimates of the neutrino luminosity (Eq. (24)) and the mean energy of neutrinos emitted from the disk, $\langle\epsilon_\nu\rangle \approx 3k_{\rm B}T_{\rm surf} \approx 11...15\,{\rm MeV}$ (Eq. (21)), agree well with our numerical results for the phase shortly after the merging. While the dynamical time scale of the merging is of the order of 1 ms and the post-merging evolution was followed by our numerical simulations for a period of about 10 ms, the disk emits neutrinos with similar luminosities for a much longer time of a few hundred milliseconds (cf. Eq. (23)). Therefore, Eq. (26) gives a number for the energy deposition by $\nu\bar{\nu}$-annihilation that is a factor of 10–100 larger than the $\sim 10^{48}$ erg calculated in Sect. 4.2.

5. Discussion

In this paper we have reported about hydrodynamical calculations of the merging of equal-mass binary neutron stars with different initial spins. We have analysed the models for their neutrino emission, for neutrino-antineutrino annihilation in the surroundings of the merger, and for the thermodynamical conditions in the merged object.

5.1. Mass loss and nucleosynthesis

The dynamical merging proceeds within a few milliseconds after the simulations were started from an initial center-to-center distance of 42 km of the two 1.6 $M_\odot$ neutron stars. Shortly after the two stars have fused into one compact object with a mass of about 3 $M_\odot$ and an average density of more than $10^{14}\,{\rm g/cm^3}$, spun-off matter forms a less dense toroidal cloud ($\rho \approx 10^{12}\,{\rm g/cm^3}$) that is heated to temperatures of 5–10 MeV by friction in shock waves and strong pressure waves sent into the surrounding gas by the oscillations and periodic pulsations of the central high-density body. Roughly 0.1 $M_\odot$ of material receive a large momentum and are pushed beyond the grid boundaries. However, only a small fraction of at most $10^{-5}...10^{-3}\,M_\odot$ of the matter has a total energy (internal plus kinetic plus gravitational) large enough to allow the gas to become unbound. In model A128 which has the best numerical resolution, in fact none of the matter can escape from the gravitational potential of the merger, in contrast to model A64 where it is several $10^{-5}\,M_\odot$. Notice, however, that energy released by the recombination of free nucleons into nuclei — an effect which is taken into account in our simulations by the use of the "realistic" equation of state of Lattimer & Swesty (1991) — and energy production by nuclear reactions proceeding in the cooling and expanding gas (Davies et al. 1994) can aid the mass ejection and could increase the unbound mass relative to our estimates.

The ejection of matter is also very sensitive to the amount of angular momentum that is present in the merging binary. The largest mass ejection was found in model B64 immediately after the merging, because the initial configuration of this model had a solid-body type rotation and thus the largest specific angular momentum in regions far away from the system axis. In contrast, model C64 showed the largest mass loss a few milliseconds later. The initial anti-spin setup of this model led to vigorous vibrations of the central body and to the outward acceleration of material some time after the two neutron stars had formed a single object. Whether and how much mass can be dynamically lost during the post-merging evolution, however, will also depend on the stability of the merged object. The central, compact core of the merger is so massive that it can be stabilized neither by internal pressure for the currently favored supranuclear equations of state, nor by its rapid rotation (for details, see Sect. 4.1.3 of Paper I). One therefore has to expect its collapse into a black hole within a few milliseconds. In case of model C64 not much matter would be expelled if the gravitational instability sets in before the large-amplitude post-merging oscillations have taken place.

The less dense cloud of gas that surrounds the massive, very dense central body is stabilized by internal pressure because its rotational velocities are significantly less than the Kepler velocity (see Fig. 12 of Paper I). When the massive core collapses into a black hole, the ambient matter will therefore be swallowed up by the black hole on a dynamical time scale of $10^{-4}...10^{-3}$ s. Only gas with a sufficiently large angular momentum will have a chance to remain in a disk or extended torus around the black hole. From there it will spiral into the black hole on the much longer time scale of viscous angular momentum transport. One can estimate that with typical orbital velocities of about $0.25c$ as found in our models, only gas at radii beyond about 44–107 km has an angular momentum that is large enough (for more information, see Sect. 4.1.3 of Paper I). This minimum orbital radius is outside of the grid boundaries of our simulations. We therefore conclude that essentially all the mass on the computational grid will disappear in a forming black hole more or less immediately, and only the $\sim$ 0.015–0.15 $M_\odot$ of material that have been swept off the grid might be able to end up in a toroidal "disk" around the central black hole. A disk mass of about $0.1\,M_\odot$ should be taken as an extreme upper limit for the considered scenario. Like the dynamically ejected mass, the amount of gas that ends up in a disk is sensitive to the initial angular momentum of the neutron star binary and to the relative times of black hole formation and mass spin-off. Last but not least, a quantitative answer seems to depend also on the numerical resolution, with the trend that better resolved models yield smaller estimates for the possible disk mass and mass ejection.

A mass of $10^{-4}...10^{-3}\,M_\odot$ that is dynamically ejected during the merging of binary neutron stars might have important implications for nucleosynthesis (Lattimer & Schramm 1974, 1976; Eichler et al. 1989). Dependent on the phase when the mass loss occurs, the expelled gas will start its expansion from different initial conditions of entropy and composition. The ejection of initially very cool, low-entropy material might be caused by the tidal interaction during the last stages of the inspiral and during the mass transfer phase of very close non-equal mass binaries. If the two components have "nearly equal" initial masses, the mass transfer is unstable and within a few orbital periods the lighter star can be completely dissipated into a thick, axially symmetric disk around the primary. Some fraction of the surface material might escape the system (Lattimer & Schramm

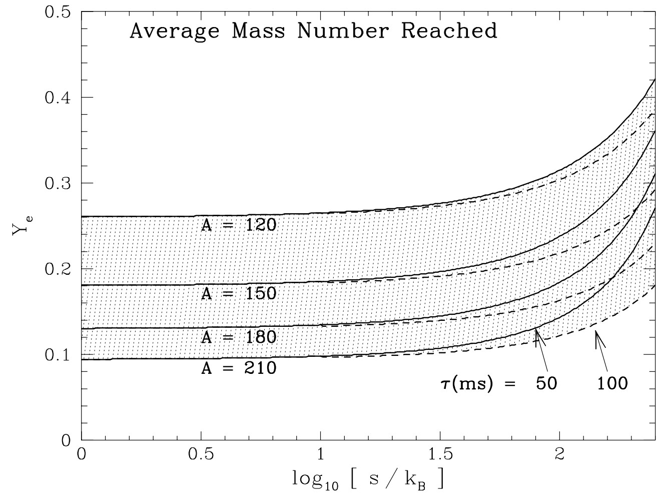

Fig. 18. Expected average mass numbers of nuclei formed by an r-process starting with NSE conditions for low entropies and with the α-process for high entropies. The plot shows contours of constant average mass number in the Y_e-s plane (s in $k_{\rm B}$ per nucleon). Y_e and s define the thermodynamical conditions in the expanding gas at a temperature of about $5 \cdot 10^9$ K, i.e., before the r-processing takes place. The dynamical evolution is characterized by the time scale τ of the adiabatic expansion between $T \sim 7 \cdot 10^9$ K and $T \sim 3 \cdot 10^9$ K. Solid lines correspond to a time scale of 50 ms, dashed lines to 100 ms. Between the contours for mass numbers $A = 120$ and $A = 210$ the shaded area marks the region where a suitably mass-weighted combination of the r-process yields for different conditions will produce a solar-system like abundance pattern. For larger values of Y_e, no significant r-processing can take place, for lower values of Y_e very strong r-processing will primarily lead to nuclei in the region of the actinides

1974, 1976). If the initial mass ratio of the two stars is large, the binary is stable against dynamical-time scale mass transfer and there is the interesting possibility that the secondary (the less massive component) is stripped to the minimum mass of stable neutron stars, at which stage it will explode (Page 1982; Blinnikov et al. 1984, 1990; Eichler et al. 1989; Colpi et al. 1989, 1991, 1993; Colpi & Rasio 1994). However, recent investigations suggest that stable mass transfer is unlikely because the initial mass of the secondary must already be very small (below $\sim 0.4\,M_\odot$; Bildsten & Cutler 1992, Kochanek 1992, Rasio & Shapiro 1994, Lai et al. 1994). In addition, an unreasonably high value of the neutron star viscosity is needed to enforce corotation and to maintain tidal locking, because stable mass transfer requires a dynamically stable Roche limit configuration which can only exist in synchronized systems with extreme mass ratios. Such systems are essentially ruled out for neutron stars (Lai et al. 1994). If mass shedding in the discussed situations occurs, it would lead to the ejection of initially cold, very low-entropy and very neutron-rich material. Subsequent radioactive β-decays of unstable, neutron-rich heavy nuclei that are present in the decompressed matter will heat the expanding gas to temperatures around 0.1 MeV, which will give rise to r-process conditions (Lattimer et al. 1977, Meyer 1989, Eichler et al. 1989).

Gas spun off the exterior parts of the dilute toroidal cloud that surrounds the compact core of the merged binary, instead, has been heated to temperatures of $\gtrsim 1$ MeV by friction during the merging and post-merging evolution. This heating has produced entropies of a few $k_{\rm B}$ per nucleon. Neutrino emission has already raised Y_e from initial values $Y_e \approx 0.02$ to slightly less neutron-rich conditions with $Y_e \approx 0.05$–0.2. The electron degeneracy is only moderate, $\eta_e \approx 2$. All these parameters are very similar to the conditions found in the shocked outer layers of the collapsed stellar core in a type-II supernova where the site of the classical r-process has been suggested (see, e.g., Hillebrandt 1978). Compared with the supernova case, the range of Y_e-values in the potentially ejected merger material is on the low side. An r-processing occurring under such neutron-rich conditions would be very efficient and should preferentially produce r-process nuclei with very high mass numbers (Fig. 18). The predominant production of high-mass r-process elements would be in concordance with the fact that one cannot expect the formation of all Galactic r-process material in the considered low-entropy ejecta. With our numerical estimates of a few $10^{-4}\,M_\odot$ for the mass loss per merger event and with the possible event rate of NS-NS and NS-BH mergers of $10^{-6}...10^{-4}$ per year per galaxy (Narayan et al. 1991, Phinney 1991, Tutukov et al. 1992 Tutukov & Yungelson 1993), which corresponds to about $10^4...10^6$ events during the lifetime of the Galaxy, only 1–100 $M_\odot$ of the $\sim 10^5\,M_\odot$ of Galactic r-process elements could be produced. But if the r-process were strong enough, all the Galactic actinides (e.g., about 40–50 $M_\odot$ of Th) might be accounted for by the material shed during neutron star merging!

However, the neutron-rich wind that is driven by neutrino energy deposition in the outer disk regions can also contribute to the nucleosynthetic input into the interstellar medium. With a total neutrino luminosity of about 10^{53} erg/s the wind will have a mass outflow rate of the order of 0.001–0.01 $M_\odot{\rm s}^{-1}$ (Qian & Woosley 1996, Woosley 1993b), depending on the gravitating mass of the merger, the disk mass and geometry, and the neutrino emission as a function of time. For a duration of the outflow between some fractions of a second and a few seconds, one might therefore have another $10^{-4}\,M_\odot$ up to several $10^{-2}\,M_\odot$ of material that are expelled with very interesting thermodynamical properties.

Like the neutrino-driven wind from new-born neutron stars, the neutrino-heated material should have significantly higher entropies than the matter that is dynamically ejected from the disk or torus by momentum transfer during core pulsations. Owing to the particularities of geometry, gravitational potential, and neutrino emission in the merger situation, the expansion time scales as well as the degree of neutronization might be significantly different from the supernova case. Since the neutrino emission from the core and the disk of the merger is dominated by the $\bar\nu_e$ fluxes, absorptions of $\bar\nu_e$ in the wind material ($\bar\nu_e + p \rightarrow n + e^+$) will be more frequent than the absorption of less abundant ν_e ($\nu_e + n \rightarrow p + e^-$) and will keep the expanding material neutron-rich. Because of a larger luminosity ratio $L_{\bar{\nu}_e}/L_{\nu_e} \approx$ 3–4.5 but similar mean ν_e and $\bar{\nu}_e$ energies with $\langle\epsilon_{\bar{\nu}_e}\rangle/\langle\epsilon_{\nu_e}\rangle \approx$ 1.5–1.8, the expanding wind will have a lower electron fraction than in the supernova case (see Qian & Woosley 1996 for a discussion of the electron fraction in neutrino-driven winds). Values as low as $Y_e \approx [1 + L_{\bar{\nu}_e}\langle\epsilon_{\bar{\nu}_e}\rangle/(L_{\nu_e}\langle\epsilon_{\nu_e}\rangle)]^{-1} \approx$ 0.1–0.2 seem possible in the neutrino wind from the merger. For such low values of Y_e a strong r-processing can happen even at modest entropies of $s \sim 50$–$100\ k_{\rm B}/\mathrm{nucleon}$ (see Sect. 5.2 for an estimate of the wind entropies) which are too low to allow for the formation of r-process nuclei in the neutrino-driven winds from protoneutron stars for the typical electron fractions of $Y_e \gtrsim$ 0.35–0.4 found there (Witti et al. 1994, Takahashi et al. 1994, Woosley et al. 1994, Qian & Woosley 1996). Figure 18 visualizes this and shows that even for rather slow expansions with expansion time scales of more than 100 ms nuclei with mass numbers A between 150 and 210 can be formed.

Unfortunately our current models allow only rough estimates of the mass loss and the conditions in the ejected matter. Our simulations could not directly follow the ejection of mass from the merger because they suffered from the limitations due to the use of the computational grid and due to an insufficient numerical resolution, especially of matter at low densities. A detailed and meaningful analysis of the very interesting aspects of a possible r-processing in the dynamically ejected low-entropy material and in the high-entropy neutrino-driven winds from NS-NS or NS-BH mergers has to be postponed until models are available which yield more quantitative information about the long-time evolution of the merged object, the torus geometry, and the neutrino-matter interactions in the outer parts of the torus. Only such models can give evidence about the duration of the mass loss and the amount of material that is ejected with different entropies, different expansion time scales, and different degrees of neutronization, all of which determine the nucleosynthetic processes (see Fig. 18 and also Woosley & Hoffman 1992, Witti et al. 1994).

5.2. Neutrino emission and gamma-ray bursts

The luminosities and mean energies of the neutrinos emitted from merging neutron stars are very similar to those calculated for supernovae and protoneutron stars. After the two neutron stars have merged, luminosities up to several 10^{52} erg/s are reached for every neutrino species and the average energies of ν_e leaking out of the merger are 10–13 MeV, of $\bar{\nu}_e$ they are 19–21 MeV, and of heavy-lepton neutrinos around 26–28 MeV. However, the neutrino emission exhibits characteristic differences from the supernova case, too.

The total neutrino luminosity from merging neutron stars does not increase to a value above 10^{52} erg/s before the hot, toroidal gas cloud around the dense and compact core of the merger starts to form. More than 90% of the peak neutrino emission of about 10^{53} erg/s stems from the "disk" region where the optical depths and thus the neutrino diffusion time scales are significantly smaller than in the core. Another pecularity is the fact that the very neutron-rich, decompressed and heated neutron star matter predominantly emits electron antineutrinos. This should hold on until the electron fraction in the medium has grown to a level where the increase of the lepton number by $\bar{\nu}_e$ emission is compensated by the ν_e losses. If the merged configuration remained stable for a sufficiently long time, the deneutronization phase will be superseded by an extended period where the heated gas deleptonizes and cools again and thus evolves back to the state of cold neutron star matter. However, it is very likely that the merged object, which contains essentially the baryonic mass of two typical neutron stars (about $3\,M_\odot$), does not remain gravitationally stable. For all currently favored nuclear equations of state it should collapse to a black hole long before the cooling is finished.

If the gravitational instability of the massive core of the merged object sets in before the hot gaseous torus has formed and if all the surrounding gas falls into the black hole immediately, the neutrino emission from the merger will stay fairly low with a total luminosity of less than $\sim 10^{52}$ erg/s. This is much too low to get sufficient energy for a cosmological gamma-ray burst from $\nu\bar{\nu}$-annihilation during the final stages of the inspiral of the two neutron stars and during the first 1–4 ms right after the merging. The annhilation efficiency of neutrinos and antineutrinos, $e_{\nu\bar{\nu}} = (\mathrm{d}E_{\nu\bar{\nu}}/\mathrm{d}t)/L_\nu$, increases proportional to the neutrino luminosity (Eq. (10)) and the neutrino energy deposition rate $E_{\nu\bar{\nu}}$ with the product of neutrino and antineutrino luminosities. At the time of maximum neutrino emission some 6–8 ms after the stars have merged, we calculate an annihilation efficiency of $(2$–$3)\cdot 10^{-3}$ and a neutrino energy deposition rate of 2–$4\cdot 10^{50}$ erg/s in the whole space outside the high-density regions of the compact core and the surrounding "disk". The integrated energy deposition during the simulated evolution of about 10 ms is therefore less than $4\cdot 10^{48}$ erg (assuming maximum neutrino fluxes during the whole considered times). Even with the unrealistic assumption that all the $\nu\bar{\nu}$-annihilation energy could be useful to power a relativistic pair-photon fireball, this energy would fail to account for the canonical $\sim 10^{51}/(4\pi)$ erg/steradian of a typical gamma-ray burst at cosmological distances (e.g., Woods & Loeb 1994; Quashnock 1996) by nearly three orders of magnitude. Of course, these arguments are not conclusive if there is strong focussing of the expanding fireball into a narrow solid angle $\delta\Omega$. In this case an observer would deduce a largely overestimated value (by a factor $4\pi/\delta\Omega$) for the energy in the fireball and in the gamma-ray burst if he assumed isotropy of the emission. However, for the considered merger scenario and the geometry of the post-merging configurations in our simulations, it is very hard to imagine how the required strong beaming of the fireball into a jet-like outflow could be achieved.

It is interesting to note that if the neutrino emission calculated for our merger models would continue for a few seconds, which is a typical duration of observed gamma-ray bursts (e.g., Norris et al. 1994, Kouveliotou 1995), a burst energy of about 10^{51} erg could well be accounted for by the annihilation of neutrinos and antineutrinos. An accretion disk or torus around the central black hole could provide a luminous neutrino source for the required period of time. This time span is much longer than the times covered by our hydrodynamical modelling. Since the current numerical simulations were neither able to mimic the effects of a central black hole nor to track the evolution of the merger for a sufficiently long time, we attempted to develop a simple analytical model in Sect. 4.3 to give us insight into the principal dependences of the energy deposition by the annihilation of neutrinos emitted from the disk or torus.

This torus model was based on Newtonian physics and did not determine the torus structure self-consistently. However, the analytic treatment took into account the effects of viscous angular momentum transport, viscous heating, neutrino cooling, and partial neutrino opaqueness. To first order and on a qualitative level, our considerations should also be valid for accretion disks around black holes in general relativity (see, e.g., Shapiro & Teukolsky 1983) and for tori around Schwarzschild black holes (see, e.g., Chakrabarti 1996). In fact, the employed assumptions about the torus geometry are supported by general relativistic investigations of neutron tori (Witt et al. 1994; Jaroszyński 1993, 1996) and the neutrino luminosities from our simple torus model are compatible with those obtained from the relativistic analyses. Moreover, the neutrino flux and neutrinospheric temperature calculated analytically are also in good agreement with the results of our numerical models for the post-merging phase when the neutrino emission has reached its saturation level.

Equation (26) gives the estimate of the $\nu\bar{\nu}$-annihilation energy $E_{\nu\bar{\nu}}$ for our analytical disk model. We find that $E_{\nu\bar{\nu}}$ could at best lie between $1.1 \cdot 10^{49}$ erg and $9.4 \cdot 10^{49}$ erg for a disk of $0.1\,M_\odot$ around a 3 $M_\odot$ black hole. The lifetime of such a disk is determined by the time scale of the outward transport of angular momentum and is estimated to be several ten up to a few hundred milliseconds. The ranges of values account for the uncertainties in the neutrino opacity (which depends on the composition of the medium and on the neutrino spectra) and for the corresponding variation of the neutrino luminosity and mean energy of the emitted neutrinos. Further uncertainties due to the unknown disk viscosity are circumvented by deriving the result for a value η^* of the dynamic shear viscosity (Eq. (20)) which assures a maximum result for $E_{\nu\bar{\nu}}$.

Unless focussing or beaming of the expanding pair-photon fireball towards the observer plays an important role, the annihilation energy of Eq. (26) is too low by more than a factor of 10 to explain powerful cosmological gamma-ray bursts. Weak bursts with an energy of about 10^{50} erg and durations of less than or around a second, however, do not seem to be completely excluded on grounds of Eqs. (26) and (23). The result of Eq. (26) and in particular the upper value of $\sim 10^{50}$ erg should be considered as a very optimistic maximum estimate for the energy deposited by $\nu\bar{\nu}$-annihilation in the surroundings of the disk. Equation (26) was derived for the most favorable conditions and by making a whole sequence of most extreme assumptions, the combination of all of which appears rather unlikely.

In the first place it was assumed that the dynamic viscosity of the disk adopts the optimum value η^* of Eq. (18). For much smaller viscosities the toroidal disk should stay rather cool and the neutrino fluxes correspondingly low. For much larger values of the viscosity the lifetime of the disk will decrease because the mass accretion rate into the black hole increases with the rate of the outward transport of angular momentum mediated by viscous forces. In this case the neutrino luminosities will be bounded by the fact that the viscous friction will heat up the disk to very high temperatures and thus the neutrino absorption and scattering cross sections, which scale roughly with the square of the neutrino energy, will increase. Therefore the neutrino diffusion time scale will increase, too, and the neutrino cooling will become inefficient. As a consequence, most of the dissipated gravitational and rotational energy could be advected into the black hole when the matter, after having lost part of its angular momentum, spirals in through the innermost stable circular orbit (advection-dominated regime).

Equation (26) also represents an optimistically high value of the energy deposition by $\nu\bar{\nu}$-annihilation because the radiation efficiency of about 8% obtained for our Newtonian model of a Keplerian accretion disk is an upper bound to the radiation efficiency of a relativistic disk around a nonrotating black hole where it is less than 6%. Moreover, it should be remembered that the annihilation efficiency $e_{\nu\bar{\nu}}$ of Eq. (10) most likely overestimates the useful fraction of the annihilation energy by a considerable factor. Our hydrodynamical simulations show that the fraction of the neutrino energy deposited in the possibly baryon-poor region above and below the disk but not in the plane of the disk (where it will serve to drive a baryonic, nonrelativistic wind instead of creating a relativistically expanding pair-photon fireball) could be as small as some 20–25% of the number given in Eq. (26) (cf. Fig. 17). Even more, general relativistic effects were neglected in the numerical simulations and analytical considerations presented here. Jaroszyński (1993) showed that they lower the energy that can be transported to infinity significantly (by about 80%).

For the whole uncertainty range of the neutrino interaction cross section (Eq. (17)) and for the corresponding range of neutrino luminosities and mean energies of emitted neutrinos, we find that the result of Eq. (26) falls short of the desired value $E_{\nu\bar{\nu}}/(4\pi) \sim 10^{51}/(4\pi)$ erg/steradian by at least an order of magnitude if the disk mass is of the order of $0.1\,M_\odot$ and the central black hole has a mass of about 3 $M_\odot$. From our numerical models of NS-NS mergers, one concludes that a disk with a mass close to or even larger than $0.1\,M_\odot$ might be formed only under very special conditions. Even if there is a high angular momentum in the system due to neutron star spins as in our model B64, the amount of material that has a chance to form a disk is hardly as much as $0.1\,M_\odot$ (see Paper I). In models A64 and C64 the lower angular momentum allows only little material to possibly remain in a disk. Only matter outside of the boundary of our computational grid has enough angular momentum to be rotationally stabilized. Before some matter in models A64 and C64 has acquired a sufficiently large angular momentum to be lost off the computational grid — a process that is partly aided by pressure waves created by the wobbling and ringing of the central, compact object — the merger, however, has probably already collapsed to a black hole which swallows up most of the surrounding, pressure supported matter on a dynamical time scale.

Massive, self-gravitating tori around black holes may be subject to general relativistic global instabilities that lead to catastrophic runaway mass loss and may provide by far the shortest evolutionary time scale of such tori as recently argued for stationary polytropic tori by Nishida et al. (1996) and for stationary neutron tori by Nishida & Eriguchi (1996). Such an instability would have the same implications as the case of extremely large disk viscosity discussed above where the accretion time scale of the torus due to the rapid viscous angular momentum transport could be much smaller than the neutrino diffusion time scale. As a consequence of the rapid accretion of the torus material, most of the internal energy of the gas would be carried into the black hole along with the gas instead of being radiated away by neutrinos. Because the duration of the neutrino emission would be very short without a compensating increase of the neutrino luminosity, the total energy emitted in neutrinos would be much smaller than in the extreme and optimum situation considered in the derivation of Eq. (26) in Sect. 4.3. Therefore, global disk instabilities might be another threat to neutrino-powered gamma-ray bursts. However, it has still to be demonstrated whether global runaway instabilities develop in the non-stationary situation and how they behave and evolve in the presence of changes of the angular momentum distribution.

Even if the lifetime of the merger and of the neutrino radiating accretion torus is long enough and neutrino annihilation could provide a powerful "engine" for creating a fireball, yet another major concern for the viability of the considered γ-ray burster scenario comes from the baryonic wind that is blown off the surface of the merger and accretion torus by neutrino heating. This neutrino-driven wind is unavoidable when large neutrino fluxes are emitted and a small fraction of these neutrinos annihilate or react with nucleons in the low-density gas in the outer layers of the merger. In order to obtain bulk Lorentz factors $\Gamma \sim \dot{E}_{\nu\bar{\nu}}/(\dot{M}_{\rm w}c^2) \gtrsim 100$ one can only allow for mass loss rates $\dot{M}_{\rm w} \lesssim 2\cdot 10^{-6}\, M_\odot {\rm s}^{-1}$ if the rate at which the pair-photon fireball is supplied with energy is $\dot{E}_{\nu\bar{\nu}} \approx 3\cdot 10^{50}$ erg/s. With about 2/3 or $\sim 2\cdot 10^{50}$ erg/s of this energy being transferred to the dilute outer regions of the accretion torus in our models (Sect. 4.2) by $\nu\bar{\nu}$-annihilation (neglecting additional heating by neutrino-electron scattering and neutrino absorption), we compute a mass loss rate of at least $\dot{M}_{\rm w} \gtrsim \frac{2}{3}\dot{E}_{\nu\bar{\nu}}\cdot [GM/(3R_{\rm s})]^{-1} \gtrsim 7\cdot 10^{-4}\, M_\odot {\rm s}^{-1}$ for a black hole with mass $M = 3\, M_\odot$ and Schwarzschild radius $R_{\rm s} \approx 27$ km. From this we get $\dot{E}_{\nu\bar{\nu}}/(\dot{M}_{\rm w}c^2) \lesssim 0.25$ and estimate an entropy $s \approx (\varepsilon + P)/(k_{\rm B}T\rho/m_{\rm u})$ (ε internal energy density, P pressure) of $s \approx \left[4m_{\rm u}c^2/(3k_{\rm B}T)\right]\left[(\dot{E}_{\nu\bar{\nu}}/3)/(\dot{M}_{\rm w}c^2)\right] \lesssim 100$–$200\ k_{\rm B}/{\rm nucleon}$ when $k_{\rm B}T \sim 0.5 \ldots 1$ MeV. Therefore, unless the neutrino-driven wind can be hindered to penetrate into the pair-photon fireball, e.g., in a region along the system axis by centrifugal forces, there is no chance to obtain highly relativistic fireballs with $\Gamma \gtrsim 100$.

These issues might also be critical when a neutron star merges with a black hole or when two non-equal mass neutron stars coalesce. Simulations indicate (Lee & Kluźniak 1995) that already after the dynamical interaction of a neutron star and a black hole a cloud of baryonic material might "pollute" the surroundings even near the system axis. Moreover, instead of an accretion torus, a stable binary system might form with a more massive black hole circulated by a low-mass neutron star companion which is possibly unstable to explosion (see also Sect. 5.1 and Blinnikov et al. 1984, Eichler et al. 1989). Future, better resolved computations covering a wider range of equations of state and masses of the interacting stars will have to show the conclusiveness of their results.

It is interesting to speculate whether there is a chance to get tori more massive than in the merging of two (nearly) equal-mass neutron stars when a neutron star merges with a black hole or when a small neutron star is tidally disrupted before merging with a companion neutron star which has a significantly larger mass (e.g., Eichler et al. 1989, Narayan et al. 1992, Mochkovitch et al. 1993, and references therein). On the one hand, a more massive disk can radiate neutrinos for a longer time than the accretion time scale of the innermost, most strongly neutrino radiating part near the last stable orbit around the black hole. With much more matter being at larger radii, the neutrino emitting torus region considered and normalized to a mass of $0.1\, M_\odot$ in the derivation of Eq. (26) will be continuously refed by material advected inward. On the other hand, Eq. (26) suggests that the energy that can be provided in the pair-photon fireball by $\nu\bar{\nu}$-annihilation increases steeply with the mass M of the central black hole, $E_{\nu\bar{\nu}} \propto R_{\rm s}^{13/8} \propto M^{13/8}$. Larger gravitating masses at the center, e.g., a massive stellar black hole, might therefore allow for more powerful γ-ray bursts, at least, if one relies on the simplified picture developed in the derivation of Eq. (26) which does not take into account the dynamics of the tidal interaction between neutron star and black hole and its implications for the disk formation and the disk mass.

For the reasons outlined above it appears to be extremely hard to account for the energies of cosmological γ-ray bursts by $\nu\bar{\nu}$-annihilation, at least in the case of merging binary neutron stars if beaming or focussing of the fireball towards the observer does not play a crucial role. The same conclusion was arrived at by Jaroszyński (1993, 1996) who investigated models of relativistic tori around rotating stellar mass black holes and tested different values of specific angular momentum, viscosity, and entropy. He found that the neutrino emission and annihilation energy from these tori is insufficient to explain the energies of cosmological γ-ray bursts except for tori around Kerr black holes with very high angular momentum, i.e., with relativistic rotation parameters $a \sim 1$. This might indeed be realized in the collapsed cores of rapidly rotating Wolf-Rayet stars in the "failed supernova" or "collapsar" scenario (Woosley 1993a). However, models for the stellar evolution of Wolf-Rayet stars seem to indicate that the angular momentum loss during the mass-loss phases is too large to allow for the formation of very rapidly spinning black holes (Langer, personal communication). Moreover, with $\nu\bar{\nu}$-annihilation as the source of the energy of the pair-photon fireball, these models might come into additional trouble if, as claimed by Quashnock (1996), the homogeneity of the distribution of the bursts in the BATSE 3B Catalog and the non-association of the bursts with large-scale structures of luminous matter in our extragalactic neighbourhood implies such large distances of the γ-ray burst sources that the required total energy output in γ-rays is larger than $3 \cdot 10^{51}$ erg.

Our investigations do not include effects due to possible convective overturn and instabilities in the disk that might occur as a result of specific entropy (or composition) inversions caused by neutrino effects or viscous heating. Such dynamical processes were recently found to be present in multi-dimensional models of type-II supernovae (Herant et al. 1994; Burrows et al. 1995; Janka & Müller 1995, 1996) and were computed for axisymmetric advection-dominated accretion flows with two-dimensional hydrodynamical simulations by Igumenshchev et al. (1996) (see also Chen 1996). Although the disk remains globally stable, shorter-wavelength modes may affect the flow dynamics and effective disk viscosity significantly. In addition, such instabilities might increase the neutrino fluxes and the average neutrino energies considerably and thus might help $\nu\bar{\nu}$-annihilation. Our three-dimensional hydrodynamical simulations were not followed for a sufficiently long time to see whether such overturn processes occur in the merging scenario, and the simplified one-zone torus model does not take into account an enhancement of the neutrino fluxes by possible convective transport. Also, magnetic fields in the merging neutron stars and in the torus were disregarded. Within a lifetime of a few tenths of a second, initial B-fields of $\sim 10^{12}$–10^{13} G might be amplified by a factor of 100 or more in the rapidly rotating disk around the black hole (rotation periods $\sim 1\,\mathrm{ms}$) and might become energetically important (Rees, personal communication). A relativistic magneto-hydrodynamical wind of extremly high luminosity, perhaps associated with a binary neutron star merger, was suggested to generate γ-ray bursts by Thompson (1994). In this respect NS-BH mergers and neutron star collisions and coalescence need further theoretical investigation. Moreover, neutron star collisions were recently pointed out as potential origin of short cosmological γ-ray bursts by Katz & Canel (1995a) who argued that hot matter fragments could be ejected and, when they become neutrino-transparent on dynamical time scales, could lead to the emission of neutrinos with very high luminosities.

6. Summary and conclusions

The neutrino emission and neutrino-antineutrino annihilation during the coalescence of binary neutron stars were investigated. To this end the three-dimensional Newtonian equations of hydrodynamics were integrated by the Riemann-solver based “Piecewise Parabolic Method” on an equidistant Cartesian grid with a resolution of $64 \times 64 \times 32$ or $128 \times 128 \times 64$ zones. The properties of neutron star matter were described by the equation of state of Lattimer & Swesty (1991). Energy loss and changes of the electron abundance due to the emission of neutrinos were taken into account by an elaborate “neutrino leakage scheme”. We have simulated the coalescence of two identical, cool (initially $k_{\mathrm{B}}T_{\mathrm{c}} \approx 7\,\mathrm{MeV}$) neutron stars with a baryonic mass of about $1.6\,M_{\odot}$, a radius of 15 km, and an initial center-to-center distance of 42 km for three different cases of initial neutron star spins.

The total neutrino luminosity prior to and during the dynamical phase of the coalescence is very small ($L_\nu \lesssim 10^{51}$ erg/s), becomes about 1–$2 \cdot 10^{52}$ erg/s when the stars have merged into one rapidly spinning massive body, and climbs to 1–$1.5 \cdot 10^{53}$ erg/s after spun off material has formed a hot toroidal cloud with a mass of 0.1–$0.2\,M_{\odot}$ around the wobbling and pulsating central object. The neutrino fluxes are clearly dominated ($\sim$90–95%) by the emission from this “disk”. Since the disk matter is neutron-rich, $\bar{\nu}_e$ are radiated with a luminosity that is a factor 3–6 higher than the (individual) luminosities of ν_e and ν_x ($\equiv \nu_\mu$, $\bar{\nu}_\mu$, ν_τ, $\bar{\nu}_\tau$). The mean energies of the emitted neutrinos are very similar to those of supernova neutrinos, $\langle\epsilon_{\nu_e}\rangle \approx 12\,\mathrm{MeV}$, $\langle\epsilon_{\bar{\nu}_e}\rangle \approx 20\,\mathrm{MeV}$, and $\langle\epsilon_{\nu_x}\rangle \approx 27\,\mathrm{MeV}$.

When the neutrino luminosities are highest, only about 0.2–0.3% of the energy emitted in neutrinos is deposited in the immediate neighborhood of the merger by $\nu\bar{\nu}$-annihilation, and the maximum integral energy deposition rate is found to be about 3–$4 \cdot 10^{50}$ erg/s. Thus, to pump an energy of the order of $10^{51}/(4\pi)$ erg/steradian into a fireball of e^+e^--pairs and photons, the strong neutrino emission would have to continue for several seconds. Since a collapse of the central core of the merger with a mass of $\gtrsim 3\,M_{\odot}$ into a black hole within milliseconds seems unavoidable, we conclude that the available energy is insufficient by a factor of about 1000 to explain gamma-ray bursts at cosmological distances. However, it appears possible that an accretion torus with a mass of ~ 0.1–$0.2\,M_{\odot}$ remains around the central black hole and is accreted on the time scale of viscous angular momentum transport. Analytical estimates suggest that even under the most favorable conditions in this torus and with an optimum value of the disk viscosity, annihilation of $\nu\bar{\nu}$ pairs emitted from this torus provides an energy that is still more than a factor of 10 too small to account for powerful cosmological gamma-ray bursts, unless focussing of the fireball expansion plays an important role.

A few $10^{-4}\,M_{\odot}$ of very neutron-rich, low-entropy matter may be dynamically ejected shortly after the neutron stars have merged, and another 10^{-4} up to a few $10^{-2}\,M_{\odot}$ of strongly neutronized, high-entropy material might be carried away from the accretion torus in a neutrino-driven wind on a time scale between a fraction of a second and a few seconds. The contamination with these baryons is a severe threat to a relativistic fireball. Aspects of nucleosynthesis in these ejecta were discussed. Because of the neutron-richness of the ejected material and the dominance of the $\bar{\nu}_e$ luminosity from the merged object and its accretion torus, conditions suitable for the formation of r-process elements might be realized more easily than in the neutrino wind from newly formed neutron stars.

It seems to be very difficult to fulfill the energetic requirements of cosmological gamma-ray bursts with the annihilation of $\nu\bar{\nu}$ pairs emitted from an accretion disk or torus around a stellar mass black hole. If $\nu\bar{\nu}$-annihilation is nevertheless to be saved as energy source for relativistic pair-photon fireballs — despite of the problems exposed by our numerical and analytical results and the critical issues addressed in the discussion of Sect. 5 — then one is forced to consider the following possibilities.

The neutrino luminosities from the accretion torus could be considerably higher than obtained in our models, but the mechanism to achieve this has yet to be identified, e.g., it is possible that the neutrino transport in the torus is enhanced by convective instabilities. Because of the quadratic dependence on the neutrino luminosities, an increase of the neutrino fluxes would affect the $\nu\bar{\nu}$-annihilation sensitively. Alternatively, still relying on the simple picture described in Sects. 4.2 and 4.3, one might feel tempted to interpret the estimates of the annihilation energy towards the optimistic side, although they were derived by employing a number of very generous and favorable assumptions. In this case some interesting implications for the hypothesis of stellar mass accretion disks around black holes as sources of gamma-ray bursts (Paczyński 1991; Narayan et al. 1992; Woosley 1993a, 1996) can be inferred from combining the theoretical results with information about measured burst time scales (Meegan et al. 1995a, Kouveliotou 1995) and energies of cosmological bursts (e.g., Woods & Loeb 1994; Quashnock 1996).

Short gamma-ray bursts have a typical duration t_γ of several tenths of a second and a typical total energy that is a factor of $\sim$ 20 smaller than that of long bursts (Mao et al. 1994). They require the release of neutrino energy from accretion tori with masses $M_{\rm d} \sim 0.1\,M_\odot\,[t_\gamma/(0.05\,...\,0.2\,{\rm s})] \sim$ few $0.1\,M_\odot$ and a beaming of the expanding fireball into a solid angle $\delta\Omega \sim 4\pi\,\left[(1\,...\,9)\cdot 10^{49}\,{\rm erg}/E_\gamma\right]\,[M_{\rm d}/0.1\,M_\odot]$, when E_γ is the typical energy of a cosmological gamma-ray burst if the gamma-rays were radiated isotropically. $\delta\Omega$ becomes smaller if the useful energy from $\nu\bar{\nu}$-annihilation is less than $(1\,...\,9)\cdot 10^{49}$ erg. For $E_\gamma \sim 10^{51}$ erg the focussing of the fireball is noticable, $\delta\Omega \sim 4\pi/10$, whereas for $E_\gamma \sim 10^{50}$ erg it is essentially absent. The required accretion mass might suggest merging events of compact binaries as the origin of the bursts in this case. The disk masses and a possible focussing of the fireball expansion towards the observer have to be explained by theoretical modelling.

For long bursts, most of which have durations t_γ between some 10 s and about 100 s, the accretion of $M_{\rm d} \sim$ few $M_\odot$ is needed and could provide an energy $E_\gamma \sim (1\,...\,9)\cdot 10^{50}\,[M_{\rm d}/M_\odot]$ erg which is of the order of $\sim 10^{51}$ erg without significant focussing of the relativistic pair-photon plasma being necessary. For more energetic bursts some beaming of the fireball expansion would have to be invoked. The large accretion mass favors the "failed supernova" or "collapsar" scenario (Woosley 1993a). In this model several solar masses of material surround the most strongly neutrino radiating region of the accretion torus close to the innermost stable orbit around the black hole. This should lead to mixing of baryons with a significant fraction of the pair-photon plasma and will confine the volume where $\nu\bar{\nu}$-annihilation might create a relativistic fireball to a baryon-poor region along the system axis. The fireball will expand into a limited solid angle which should compensate for the reduction of the useful fraction of the $\nu\bar{\nu}$-annihilation energy.

This interpretation of the bimodal distribution of burst durations (Kouveliotou et al. 1993) employs two different kinds of astrophysical events. In contrast, Wang (1996) attempted to explain the bimodality by a superposition of two distinct time scales in the temporal structure of individual bursts corresponding to peak widths and separations between adjacent peaks. Katz & Canel (1995a,b) have recently suggested the association of short and long bursts with two different classes of models and have hypothesized that short bursts are produced by neutron star collisions and long bursts originate from accretion-induced collapse of bare degenerate white dwarfs (Dar et al. 1992). In both types of models the burst energy would be provided by the annihilation of emitted $\nu\bar{\nu}$ pairs. Accretion induced collapse, however, was ruled out as a source of gamma-ray bursts situated at cosmological distances by Woosley & Baron (1992) on grounds of the unacceptably large baryonic pollution of the surroundings of the collapsed star caused by a nonrelativistic neutrino-driven wind. The same worries also hold for collisions of neutron stars where explosions of ejected low-mass fragments might create an envelope of baryonic material around the collision site. Moreover, one has to be suspicious whether the neutrino emission will be luminous and long enough that $\nu\bar{\nu}$-annihilation can provide an energy $\gtrsim 10^{50}$ erg for a short and most likely unbeamed gamma-ray burst.

Neutrino emission and $\nu\bar{\nu}$-annihilation would be the energy source for the gamma-ray bursts also in the two classes of models that could lead to accretion tori around black holes, i.e., the merging of binary neutron stars or of neutron star black hole systems in case of short bursts, and collapsing, very massive stars which do not succeed to explode as type-II supernovae in case of long bursts. The bimodal distribution of burst durations would reflect the two distinct mass ranges of the accretion tori around the accreting stellar mass black holes, some $0.1\,M_\odot$ or a few $M_\odot$, respectively. The similar peak luminosities of both short and long bursts (Mao et al. 1994) could be explained by the same underlying energy source for the gamma-ray bursts. The short-time variability of the gamma-ray signal could be a consequence of jet precession (Hartmann & Woosley 1995) or of inhomogeneities and instabilities in the accretion torus that give rise to fluctuations of the accretion rate. And the individual characteristics of burst events might be associated with different masses of accretion tori and accreting black holes, different torus structures due to different angular momentum distributions, and different accretion time scales because of variations of the angular momentum transport, e.g., caused by magnetic fields or viscosity producing dissipative processes in the torus.

Movies in mpeg format of the dynamical evolution of all models are available in the WWW at `http://www.mpa-garching.mpg.de/~mor/nsgrb.html`

Acknowledgements. It is a pleasure for us to thank Wolfgang Keil for transforming Lattimer & Swesty's FORTRAN equation of state into a usable table. H.-T.J. and K.T. are very grateful to Josef Witti for extended network calculations of the α-process and for providing comfortable tools to visualize and scan the rich data base of results. M.R. would like to thank Sabine Schindler for her patience in their common office. Educative discussions with M. Camenzind, W. Hillebrandt, F. Meyer, M. Rees, and S. Woosley are acknowledged. K.T. was supported by the "Sonderforschungsbereich 375-95 für Astro-Teilchenphysik" of the Deutsche Forschungsgemeinschaft, M.R. by the Deutsche Agentur für Raumfahrtangelegenheiten (DARA), Förderungsvorhaben des Bundes, FKZ: 50 OR 92095. The calculations were performed at the Rechenzentrum Garching on a Cray-YMP 4/64 and a Cray-EL98 4/256.

References

Band D., Matteson J., Ford L., et al., 1993, ApJ 413, 281
Bildsten L., Cutler C., 1992, ApJ 400, 175
Blanchet L., Damour T., Schäfer G., 1990, MNRAS 242, 289
Blinnikov S.I., Novikov I.D., Perevodchikova T.V., Polnarev A.G., 1984, Sov. Astron. Lett. 10, 177
Blinnikov S.I., Imshennik V.S., Nadezhin D.K., Novikov I.D., Perevodchikova T.V., Polnarev A.G., 1990, Sov. Astron. 34, 595
Bloom J.S., Fenimore E.E., in 't Zand J., 1996, in: *Proc. 3rd Huntsville Gamma-Ray Burst Symposium*, Alabama, eds. C. Kouveliotou, M.S. Briggs and G.J. Fishman, AIP, in press
Brainerd J.J., Meegan C.A., Briggs M.S., Pendleton G.N., Brock M.N., 1995, ApJ 441, L39
Bruenn S.W., 1993, in: *Nuclear Physics in the Universe*, eds. M.W. Guidry and M.R. Strayer, IOP, Bristol, p. 31
Bruenn S.W., Mezzacappa A., Dineva T., 1995, Phys. Rep. 256, 69
Burrows A., Hayes J.F., Fryxell B.A., 1995, ApJ 450, 830
Cavallo G., Rees M.J., 1978, MNRAS 183, 359
Centrella J.M., McMillan S.L.W., 1993, ApJ 416, 719
Chakrabarti S.K., 1996, Phys. Rep. 266, 229
Chen X., 1996, talk presented at the Workshop *Basic Physics of Accretion Disks*, Kyoto Oct. 1995, astro-ph/9601116
Clarke T.E., Blaes O., Tremaine S., 1994, AJ 107, 1873
Colella P., Woodward P.R., 1984, JCP 54, 174
Colella P., Glaz H.M., 1985, JCP 59, 264
Colpi M., Shapiro S.L., Teukolsky S.A., 1989, ApJ 339, 318
Colpi M., Shapiro S.L., Teukolsky S.A., 1991, ApJ 369, 422
Colpi M., Shapiro S.L., Teukolsky S.A., 1993, ApJ 414, 717
Colpi M., Rasio F.A., in: *Evolutionary Links in the Zoo of Interacting Binaries*, ed. F. D'Antona et al., Memorie della Societ Astronomica Italiana, Vol. 65, 379
Cooperstein J., van den Horn L.J., Baron E.A., 1987, ApJ 321, L129
Cutler C., Flanagan E.E., 1994, Phys. Rev. 49, 2658
Dar A., Kozlovsky B.Z., Nussinov S., Ramaty R., ApJ 388, 164
Davies M.B., Benz W., Piran T., Thielemann F.K., 1994, ApJ 431, 742
Dermer C.D., Weiler T.J., 1995, Ap&SS 231, 377
Duncan R.C., Shapiro S.L., Wasserman I, 1986, ApJ 309, 141
Efron B., Petrosian V., 1995, ApJ 449, 216
Eichler D., Livio M., Piran T., Schramm D.N., 1989, Nat 340, 126
Fenimore E.E., 1996, in: *Proc. 3rd Huntsville Gamma-Ray Burst Symposium*, Alabama, eds. C. Kouveliotou, M.S. Briggs and G.J. Fishman, AIP, in press
Fenimore E.E., Epstein R.I., Ho C., 1993, A&AS 97, 59
Fishman G.J., Meegan C.A., Wilson R.B., et al., 1994, ApJS 92, 229
Fryxell B.A., Müller E., Arnett D., 1989, Max-Planck-Institut für Astrophysik Report 449, Garching, Germany
Goodman J., 1986, ApJ 308, L47
Goodman J., Dar A., Nussinov S., 1987, ApJ 314, L7
Greiner J., 1995a, Ann. NY Acad. Sci. 759, 429
Greiner J., 1995b, talk presented at the Frascati Workshop 1995 on the *Multifrequency Behavior of High-Energy Cosmic Sources*, Vulcano, May 1995, to appear in Mem. S.A. It., astro-ph/9510015
Halzen F., 1996, talk presented at the *Venitian Neutrino Conference*, Feb. 1996, Univ. of Madison report MADPH-96-937, astro-ph/9605014
Halzen F., Jaczko G., 1996, Univ. of Madison report MADPH-96-929, astro-ph/9602038
Harding A.K., 1994, in: *The Second Compton Symposium*, eds. C.E. Fichtel, N. Gehrels and J. Norris, AIP Conf. Proc. 304, New York, p. 30
Hartmann D.H., Woosley S.E., 1995, Adv. Space Res. 15, 143
Hartmann D.H., Briggs M.S., Mannheim K., 1996, in: *Proc. 3rd Huntsville Gamma-Ray Burst Symposium*, Alabama, eds. C. Kouveliotou, M.S. Briggs and G.J. Fishman, AIP, in press, astro-ph/9601057
Herant M., Benz W., Hix W.R., Fryer C.L., Colgate S.A., 1994, ApJ 435, 339
Hernanz M., Isern J., Martin X., Mochkovitch R., 1994, ApJS 92, 627
Hillebrandt W., 1978, SSR 21, 639
Hurley K., Dingus B.L., Mukherjee R., et al., 1994, Nat 372, 652
Igumenshchev I.V., Chen X., Abramowicz M.A., 1996, MNRAS 278, 236
Imshennik V.S., Popov D.V., 1994, Astron. Lett. 20, 529
Iyer B.R., Will C.M., 1993, Phys. Rev. Lett. 70, 113
Janka H.-Th., 1991, A&A 244, 378
Janka H.-Th., Müller E., 1995, Phys. Rep. 256, 135
Janka H.-Th., Müller E., 1996, A&A 306, 167
Janka H.-Th., Ruffert M., 1996, A&A 307, L33
Jaroszyński M., 1993, Acta Astron. 43, 183
Jaroszyński M., 1996, A&A 305, 839
Katz J.I., Canel L.M., 1995a, "The Long and the Short of Gamma-Ray Bursts", astro-ph/9512160
Katz J.I., Canel L.M., 1995b, "Two Classes of Gamma-Ray Bursts", astro-ph/9512074
Kochanek C.S., 1992, ApJ 398, 234
Kolatt T., Piran T., 1996, "New Evidence for the Cosmological Origin of Gamma-Ray Bursts", astro-ph/9605025
Kouveliotou C., Meegan C.A., Fishman G.J., et al., 1993, ApJ 413, L101
Kouveliotou C., 1995, Ann. NY Acad. Sci. 759, 411
Lai D., Rasio F.A., Shapiro S.L., 1993, ApJ 406, L63
Lai D., Rasio F.A., Shapiro S.L., 1994, ApJ 420, 811
Lai D., 1994, MNRAS 270, 611
Lamb D.Q., 1995, in: *75th Anniversary Astronomical Debate*, PASP 107, 1152
Lamb D.Q., 1996, in: *Proc. 3rd Huntsville Gamma-Ray Burst Symposium*, Alabama, eds. C. Kouveliotou, M.S. Briggs and G.J. Fishman, AIP, in press
Larson S.B., McLean I.S., Becklin E.E., 1996, ApJ 460, L95
Lattimer J.M., Mackie F., Ravenhall D.G., Schramm D.N., 1977, ApJ 213, 225
Lattimer J.M., Schramm D.N., 1974, ApJ 192, L145
Lattimer J.M., Schramm D.N., 1976, ApJ 210, 549
Lattimer J.M., Swesty F.D., 1991, Nucl. Phys. A535, 331
Lee W.H., Kluźniak W., 1995, Acta Astron. 45, 705
Lincoln C.W., Will C.M., 1990, Phys. Rev. D 42, 1123
Lipunov V.M., Postnov K.A., Prokhorov M.E., Panchenko I.E., Jørgensen H.E., 1995, ApJ 454, 593
LoSecco J.M., 1994, ApJ 425, 217

Mao S., Narayan R., Piran T., 1994, ApJ 420, 171
Mayle R.W., Wilson J.R., Schramm D.N., 1987, ApJ 318, 288
Meegan C.A., Fishman G.J., Wilson R.B., et al., 1992, Nat 359, 217
Meegan C.A., Pendleton G.N., Briggs M.S., et al., 1995a, ApJS, in press
Meegan C.A., Hartmann D.H., Brainerd J.J., et al., 1995b, ApJ 446, L15
Mészáros P., 1995, Ann. NY Acad. Sci. 759, 440
Mészáros P., Rees M.J., 1992a, MNRAS 257, 29P
Mészáros P., Rees M.J., 1992b, ApJ 397, 570
Mészáros P., Rees M.J., 1993, ApJ 405, 278
Mészáros P., Laguna P., Rees M.J., 1993, ApJ 415, 181
Meyer B.S., 1989, ApJ 343, 254
Mochkovitch R., Hernanz M., Isern J., Martin X., 1993, Nat 361, 236
Mochkovitch R., Heranz M., Isern J., Loiseau S., 1995a, A&A 293, 803
Mochkovitch R., Maitia V., Marques R., 1995b, Ap&SS 231, 441
Myra E.S., Burrows A., 1990, ApJ 364, 222
Nakamura T., Oohara K., 1989, Prog. Theor. Phys. 82, 1066
Nakamura T., Oohara K., 1991, Prog. Theor. Phys. 86, 73
Narayan R., Piran T., Shemi A., 1991, ApJ 379, L17
Narayan R., Paczyński B., Piran T., 1992, ApJ 395, L83
Nemiroff R.J., 1994a, Comments Astrophys. 17, 189
Nemiroff R.J., 1994b, in: *Gamma-Ray Bursts*, eds. G.J. Fishman, J. Brainerd and K. Hurley, AIP Conf. Proc. 307, New York, p. 730
Nishida S., Lanza A., Eriguchi Y., Abramowicz M.A., 1996, MNRAS 278, L41
Nishida S., Eriguchi Y., 1996, ApJ 461, 320
Norris J.P., Nemiroff R.J., Scargle J.D., et al., 1994, ApJ 424, 540
Oohara K., Nakamura T., 1989, Prog. Theor. Phys. 82, 535
Oohara K., Nakamura T., 1990, Prog. Theor. Phys. 83, 906
Paczyński B., 1986, ApJ 308, L43
Paczyński B., 1990, ApJ 363, 218
Paczyński B., 1991, Acta Astron. 41, 257
Paczyński B., 1995, in: *75th Anniversary Astronomical Debate*, PASP 107, 1167
Paczyński B., Xu G., 1994, ApJ 427, 708
Page D.N., 1982, Phys. Lett. 91A, 201
Phinney E.S., 1991, ApJ 380, L17
Piran T., 1990, in: *Supernovae*, eds. J.C. Wheeler, T. Piran and S. Weinberg, World Scientific, Singapore, p. 303
Piran T., 1995, in: *Some Unsolved Problems in Astrophysics*, Princeton, April 1995, eds. J.N. Bahcall and J. Ostriker, in press, astro-ph/9507114
Piran T., 1996, in: *Compact Stars in Binaries*, Proc. IAU Symp. 165, eds. J. van Paradijs, E.P.J. van den Heuvel, and E. Kuulkers, Kluwer, Dordrecht, p. 489
Piran T., Narayan R., Shemi A., 1992, in: *Gamma-Ray Bursts*, eds. W.S. Paciesas and G.J. Fishman, AIP Conf. Proc. 265, New York, p. 149
Podsiadlowski P., Rees M.J., Ruderman M., 1995, MNRAS 273, 755
Qian Y.-Z., Woosley S.E., 1996, ApJ, in press
Quashnock J.M., 1996, ApJ 461, L69
Rasio F.A., Shapiro S.L., 1994, ApJ 432, 242
Rees M.J., Mészáros P., 1992, MNRAS 258, 41P
Rees M.J., Mészáros P., 1994, ApJ 430, L93
Ruffert M., 1992, A&A 265, 82
Ruffert M., Janka H.-Th., Schäfer G., 1996, [Paper I], A&A 311, 532
Sari R., Piran T., 1995, ApJ 455, L143
Shapiro S.L., Teukolsky S.A., 1983, *Black Holes, White Dwarfs and Neutron Stars*, Wiley, New York
Shemi A., 1994, MNRAS 269, 1112
Shemi A., Piran T., 1990, ApJ 365, L55
Shibata M., Nakamura T., Oohara K., 1992, Prog. Theor. Phys. 88, 1079
Shibata M., Nakamura T., Oohara K., 1993, Prog. Theor. Phys., 89, 809
Smolsky M.V., Usov V.V., 1996, ApJ 461, 858
Takahashi K., Witti J., Janka H.-Th., 1994, A&A 286, 857
Teegarden B.J., 1995, Ap&SS 231, 137
Tegmark M., Hartmann D.H., Briggs M.S., Meegan C.A., 1995, ApJ, in press, astro-ph/9510129
Thompson C., 1994, MNRAS 270, 480
Thorne K., 1992, in: *Recent Advances in General Relativity*, eds. A. Janis and J. Porter, Birkhäuser, Boston, p. 196
Tutukov A.V., Yungelson L.R., Iben I., 1992, ApJ 386, 197
Tutukov A.V., Yungelson L.R., 1993, MNRAS 260, 675
Usov V.V., 1992, Nat 357, 472
Vrba F.J., 1996, in: *Proc. 3rd Huntsville Gamma-Ray Burst Symposium*, Alabama, eds. C. Kouveliotou, M.S. Briggs and G.J. Fishman, AIP, in press
Wang V.C., 1996, in: *Proc. 3rd Huntsville Gamma-Ray Burst Symposium*, Alabama, eds. C. Kouveliotou, M.S. Briggs and G.J. Fishman, AIP, in press
Weiler T.J., Simmons W.A., Pakvasa S., Learned, J.G., 1994, hep-ph/9411432
Witt H.J., Jaroszyński M., Haensel P., Paczyński B., Wambsganss J., 1994, ApJ 422, 219
Witti J., Janka H.-Th., Takahashi K., 1994, A&A 286, 841
Woods E., Loeb A., 1994, ApJ 425, L63
Woosley S.E., 1993a, ApJ 405, 273
Woosley S.E., 1993b, A&AS 97, 205
Woosley S.E., 1996, in: *Proc. 3rd Huntsville Gamma-Ray Burst Symposium*, Alabama, eds. C. Kouveliotou, M.S. Briggs and G.J. Fishman, AIP, in press
Woosley S.E., Baron E., 1992, ApJ 391, 228
Woosley S.E., Hoffman R.D., 1992, ApJ 395, 202
Woosley S.E., Wilson J.R., Mathews G.J., Hoffman R.D., Meyer B.S., 1994, ApJ 433, 229
Zhuge X., Centrella J.M., McMillan L.W., 1994, Phys. Rev. D 50, 6247

This article was processed by the author using Springer-Verlag LaTeX A&A style file *L-AA* version 3.